Neural Network-Based Adaptive Antiswing Control of an Underactuated Ship-Mounted Crane With Roll Motions and Input Dead Zones

Tong Yang, Ning Sun, *Member, IEEE*, He Chen, and Yongchun Fang, *Senior Member, IEEE*

***Abstract*— As a type of indispensable oceanic transportation tools, ship-mounted crane systems are widely employed to transport cargoes and containers on vessels due to their extraordinary flexibility. However, various working requirements and the oceanic environment may cause some uncertain and unfavorable factors for ship-mounted crane control. In particular, to accomplish different control tasks, some plant parameters (e.g., boom lengths, payload masses, and so on) frequently change; hence, most existing model-based controllers cannot ensure satisfactory control performance any longer. For example, inaccurate gravity compensation may result in positioning errors. Additionally, due to ship roll motions caused by sea waves, residual payload swing generally exists, which may result in safety risks in practice. To solve the above-mentioned issues, this paper designs a neural network-based adaptive control method that can provide effective control for both actuated and unactuated state variables based on the original nonlinear ship-mounted crane dynamics without any linearizing operations. In particular, the proposed update law availably compensates parameter/structure uncertainties for ship-mounted crane systems. Based on a 2-D sliding surface, the boom and rope can arrive at their preset positions in *finite* time, and the payload swing can be completely suppressed. Furthermore, the problem of nonlinear input dead zones is also taken into account. The stability of the equilibrium point of all state variables in ship-mounted crane systems is theoretically proven by a rigorous Lyapunov-based analysis. The hardware experimental results verify the practicability and robustness of the presented control approach.**

***Index Terms*— Antiswing control, motion control, neural networks, ship-mounted cranes, underactuated systems.**

I. Introduction

INDUSTRIAL crane systems are widely applied in the field of cargo/container transportation, which are a class of representative nonlinear systems [1]–[6], and can be divided into different types according to their various structures, such as overhead cranes, rotary cranes, tower cranes, and so on. Furthermore, for crane systems, there exist unactuated state variables (e.g., payload swing angles), which hence makes them typically underactuated systems [7]–[9], whose degrees of freedom (DoFs) are more than the number of control inputs. Consequently, the difficulty of designing control methods is further greatly increased. At present, the above-mentioned open challenging problems have attracted considerable attention; moreover, many effective controllers have been proposed, which mainly include input shaping-based control [10], trajectory planning-based control [11]–[13], adaptive control [14]–[16], sliding mode-based control [17], [18], intelligent control [19]–[21], model predictive control [22], and so forth.

With the development of marine operations, underactuated ship-mounted crane systems, which can transport payloads to preset positions, are playing more and more important roles in practice. For example, currently, the deployments of marine equipment, such as buoys and underwater robots, highly rely on ship-mounted cranes that are manually manipulated by multiple workers. However, low working efficiency and potential safety risks of human factors will significantly increase time and economic costs. Hence, addressing the above-mentioned problems through effective automatic control strategies is urgently needed. However, different from land-fixed cranes (see [1]–[21]), wave-induced loads unavoidably excite ship roll motions, which is the primary problem for marine lifting operations in the sea environment, and further result in residual payload swing around the desired position on vessels. Generally, under five-level sea conditions, the observed wave height may reach more than 2.5–4.0 m [23]. As a result, how to transport payloads to destinations in such sea conditions and suppress their residual swing are quite challenging and meaningful in real applications. Additionally, since plant parameters and structures of ship-mounted cranes are usually difficult to accurately obtain in practice, some model-based control approaches cannot guarantee satisfactory control performance in the case of parameter/structure uncertainties, which is another interesting/valuable one that deserves to be investigated deeply. Specifically, on the one hand, it is quite difficult to accurately derive the inherent characteristics (i.e., unmodeled dynamics) of practical ship-mounted crane systems. On the other hand, some physical parameters, e.g., boom

Manuscript received June 23, 2018; revised November 14, 2018 and March 13, 2019; accepted April 1, 2019. Date of publication May 6, 2019; date of current version February 28, 2020. This work was supported in part by the National Natural Science Foundation of China under Grant 61873134 and Grant U1706228, in part by the Young Elite Scientists Sponsorship Program by Tianjin under Grant TJSQNTJ-2017-02, and in part by the Fundamental Research Funds for the Central Universities under Grant 63191718 and Grant 63191512. *(Corresponding author: Ning Sun.)*

The authors are with the Institute of Robotics and Automatic Information Systems (IRAIS), College of Artificial Intelligence, Nankai University, Tianjin 300350, China, and also with the Tianjin Key Laboratory of Intelligent Robotics (tjKLIR), Nankai University, Tianjin 300350, China (e-mail: sunn@nankai.edu.cn).

Color versions of one or more of the figures in this article are available online at http://ieeexplore.ieee.org.

Digital Object Identifier 10.1109/TNNLS.2019.2910580

lengths and cargo masses, are always changing in different control tasks, which may introduce a series of control issues and limit the application ranges of most existing schemes. Currently, some intelligent learning algorithms, e.g., neural network methods [24], [25], fuzzy logic methods [26], and reinforcement learning methods [27], are introduced into controllers to handle model uncertainties of nonlinear systems. However, in most cases, a few of them can be directly applied to underactuated systems to achieve effective *full-state* control.

Due to the aforementioned important research motivation, at present, researchers are beginning to focus on ship-mounted cranes with wave-induced loads. The impact of sea waves on the dynamics of container cranes is taken into account in [28]. Moreover, a meaningful method [29] is proposed to simultaneously address heave motions and realize antiswing control. Similarly, some prediction algorithms [30], [31] are used to compensate vessel vertical motions. Furthermore, to minimize the relative vertical velocities between sea waves and payloads, a control strategy [32] is presented by wave-amplitude measurements. In addition, some sliding mode-based controllers [33], [34] are applied to ship-mounted crane systems to effectively accomplish control tasks. By using payload swing angle feedback, a command shaping method [35] can achieve swing suppression. Additionally, some effective closed-loop feedback control schemes [36]–[38] are presented to fulfill positioning control and swing elimination simultaneously.

Based on the foregoing analysis, it is not difficult to find that there are still many issues that need to be solved for ship-mounted cranes, which can be drawn as follows.

1) Most existing controllers for ship-mounted cranes are designed based on *exact model knowledge*, that is, some crane plant parameters are involved in the feedback control laws. However, in most cases, plant parameters (e.g., payload masses) may be different in various control tasks, and they are difficult to be accurately measured in practical applications; hence, the control performance may be degraded to a great extent. For example, inaccurate gravity compensation [39] unavoidably results in unfavorable boom positioning errors for cranes.
2) Generally, input dead zones of practical servo motors are common and inevitable in electromechanical systems, including multi-input ship-mounted crane systems. Nevertheless, for facilitating a ship-mounted crane controller design, the dead-zone effects are usually roughly neglected, which may deteriorate the control performance and even lead to instability. For example, limit cycles may be caused by dead zones in practical nonlinear systems [40]. Additionally, in some cases, the local stability of the system equilibrium point may be deteriorated due to actuator dead zones [41].
3) Most existing control approaches can only yield ultimate uniform boundedness (see [42], [43]) or asymptotic stability results (see [33], [44]) for the equilibrium point of complicated ship-mounted crane systems, and it is difficult to strictly guarantee the convergence time of the error signals.
4) In addition, a common way to address the control problems of nonlinear ship-mounted crane systems is to linearize original nonlinear dynamic models, which may ignore some important characteristics of practical mechanical platforms and influence the control results.

To address the above-mentioned problems, this paper presents a nonlinear control method to achieve accurate boom/rope positioning in finite time and simultaneously ensure payload swing suppression in the presence of ship roll motions (induced by sea waves) and input dead-zone effects, and it does not require the exact knowledge of plant parameters. The effectiveness and robustness of the proposed method are validated by hardware experiments. Compared with the existing control methods for ship-mounted cranes, some main works of this paper can be summarized as follows.

1) In practice, ship-mounted crane systems always suffer from some unavoidable problems, e.g., parameter uncertainties, input dead-zones, and so on, which may badly impact the control performance. Hence, in this paper, we introduce the double-layer neural network into the proposed controller to systematically address these issues, such that the boom/rope positioning errors are effectively averted and the system robustness is greatly improved. Moreover, the condition of linear parameterization (LP) can be relaxed, which is of great significance in real applications.
2) In this paper, we first ensure that the presented sliding surface can converge to zero in finite time and maintain stability, that is, the boom and rope are both steered to their desired positions in finite time. Hence, the working efficiency and operation safety are successfully guaranteed. Apart from that, rapid payload swing elimination is also achieved, which is proven by a series of rigorous theoretical analysis. As a result, the proposed controller can accomplish effective *full-state* control for ship-mounted crane systems.
3) There are no linearizing manipulations around the equilibrium point for ship-mounted cranes' originally complicated nonlinear dynamics during the process of controller design and theoretical analysis; for example, one *no longer* needs to assume that the payload swing is sufficiently small. Hence, the feasibility of the proposed controller can be ensured in the presence of large payload swing angles induced by unfavorable external disturbances.
4) In addition to theoretical analysis, we also validate the effectiveness and robustness of the proposed control scheme with hardware experiments.
5) Currently, different from fully actuated systems [45]–[48], it is difficult to prove the convergence of unactuated state variables by neural network-based controllers due to the lack of control inputs. For this issue, this paper presents some new analysis to prove that all state variables of ship-mounted crane systems are asymptotically stable at the equilibrium point. Specifically, the convergence of the unactuated variable (i.e., the payload swing angle) is strictly proven by utilizing Lyapunov-based techniques and the property of

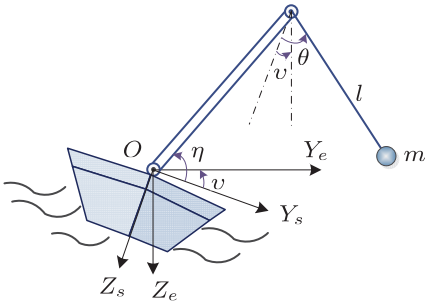

Fig. 1. Illustration of a ship-mounted crane system.

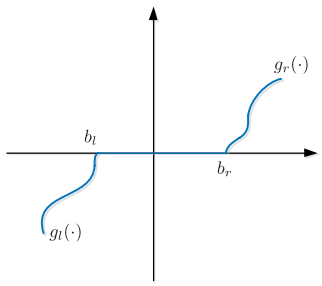

Fig. 2. Illustration for input dead-zone effects.

TABLE I
VARIABLES AND PARAMETERS OF SHIP-MOUNTED CRANES

Variables/parameters	Physical meaning	Units
$\eta(t)$	boom pitch angle in the ship-fixed frame	rad
$l(t)$	rope length	m
$\theta(t)$	payload swing angle in the ship-fixed frame	rad
$\upsilon(t)$	ship roll motion	rad
m	payload mass	kg
L_b	boom length	m
M_{ob}	product of the boom mass and the distance between the boom barycenter and point O	kg·m
J	inertia moment of the boom	kg·m^2
g	gravitational constant	m/s^2
$f_{r1}(t), f_{r2}(t), f_{r3}(t)$	influences induced by ship roll motions	N·m
$u_1(t), u_2(t)$	original control input signals calculated by control laws	N·m, N
$Z(u_1), Z(u_2)$	ultimate control torque/force due to dead-zone nonlinearity	N·m, N

converging input bounded state (CIBS), which provides some *promising* hints for applying neural networks to (other) underactuated systems.

The remaining parts of this paper are organized as follows. Sections II-A and II-B first present the dynamic model of ship-mounted crane systems and the corresponding control task, and then, a nonlinear neural network-based controller is proposed in Section III. Next, Section IV proves the convergence of all state variables by a strict stability analysis. In addition, a series of hardware experiments in Section V verifies the practicability and robustness of the proposed control scheme. Finally, Section VI sums up the entire paper.

II. PROBLEM FORMULATION

A. Ship-Mounted Crane Dynamics

The diagram (postback) of ship-mounted crane systems is shown in Fig. 1, where there are two frames [23] [i.e., the north-east-down (NED) frame Y_e–O–Z_e and the ship-fixed frame Y_s–O–Z_s, respectively], and the O–X_e axis and O–X_s axis both direct from aft to fore; moreover, the corresponding system parameters are illustrated in Table I. Before establishing dynamic models for ship-mounted crane systems, some assumptions are made as follows: 1) the lift wire is modeled as a rod; hence, the lift wire elongation and the elastic potential energy are neglected; 2) the wire elongation is always positive and snatch loads do not occur; 3) only the roll motion is considered in this paper; however, the 6-DoF motions are coupled, i.e., heave and sway motions also influence the payload a lot; 4) the payload does not influence the vessel; and 5) the wind-induced loads acting on the payload are neglected.

In this paper, we establish Lagrange's equations in the ship-fixed (noninertial) coordinate frame, where the additional torque caused by the wave-induced ship roll motion is introduced as a kind of inertial force [49]. After a series of calculations, we can derive the dynamic equations of ship-mounted cranes as follows:

$$\begin{aligned}&\left(J+mL_b^2\right)\ddot{\eta}-mL_bC_{\theta-\eta}\ddot{l}+mlL_bS_{\theta-\eta}\ddot{\theta}+2mL_bS_{\theta-\eta}\dot{l}\dot{\theta}\\&\quad+mlL_bC_{\theta-\eta}\dot{\theta}^2+(mL_b+M_{ob})gC_{\eta-\upsilon}\\&=Z(u_1)+f_{r1}\qquad(1)\\&\quad-mL_bC_{\theta-\eta}\ddot{\eta}+m\ddot{l}-mL_bS_{\theta-\eta}\dot{\eta}^2-ml\dot{\theta}^2-mgC_{\theta-\upsilon}\\&=Z(u_2)+f_{r2}\qquad(2)\\&mlL_bS_{\theta-\eta}\ddot{\eta}+ml^2\ddot{\theta}-mlL_bC_{\theta-\eta}\dot{\eta}^2+2ml\dot{l}\dot{\theta}\\&\quad+mglS_{\theta-\upsilon}=f_{r3}\qquad(3)\end{aligned}$$

where

$$\begin{aligned}f_{r1}&=\left(J+mL_b^2+mlL_bS_{\theta-\eta}\right)\ddot{\upsilon}+2mL_b\dot{l}S_{\theta-\eta}\dot{\upsilon}\\&\quad-mlL_bC_{\theta-\eta}(\dot{\upsilon}^2-2\dot{\theta}\dot{\upsilon})\\f_{r2}&=ml(\dot{\upsilon}^2-2\dot{\theta}\dot{\upsilon})+mL_bS_{\theta-\eta}(\dot{\upsilon}^2-2\dot{\theta}\dot{\upsilon})-mL_bC_{\theta-\eta}\ddot{\upsilon}\\f_{r3}&=-c(\dot{\theta}-\dot{\upsilon})+ml(l+L_bS_{\theta-\eta})\ddot{\upsilon}+mlL_bC_{\theta-\eta}\\&\quad\times(\dot{\upsilon}^2-2\dot{\theta}\dot{\upsilon})+2ml\dot{l}\dot{\upsilon}.\end{aligned}\qquad(4)$$

S_{a-b} and C_{a-b} are introduced to stand for $\sin(a-b)$ and $\cos(a-b)$ throughout this paper for brevity, respectively. Moreover, the rope length l is always positive and has the upper and lower boundaries, i.e., $\bar{l}$ and $\underline{l}$, respectively. In addition, since input dead zones (see Fig. 2) exist in practical servo motors, $Z(u_1)$ and $Z(u_2)$ denote the real input force and torque applied to ship-mounted crane systems, respectively, which can be defined as

$$Z(u_i)\triangleq\begin{cases}g_l(u_i-b_l), & u_i\le b_l\\0, & b_l<u_i<b_r\\g_r(u_i-b_r), & u_i\ge b_r\end{cases}\quad(i=1,2)\qquad(5)$$

where b_l and b_r denote the lower and upper bounds of the dead zone, respectively, and $g_l(\cdot)$ and $g_r(\cdot)$ are both unknown nonlinear functions related to dead-zone characteristics. For the

convenience of controller design, we define $Z(u_1) \triangleq u_1 + \Delta u_1$ and $Z(u_2) \triangleq u_2 + \Delta u_2$.

B. Dynamics Analysis and Control Task

Next, we carry out some analysis for the crane dynamics. To achieve positioning and antiswing control of ship-mounted crane systems, the main control objective is to transport the payload to the desired position and eliminate its residual swing in the NED coordinate frame. Hence, in this paper, we employ the position vector and motion trajectory in the NED coordinate frame to describe the payload kinematics as follows:

$$\begin{aligned}\vec{r} &= [l\sin(\theta-\upsilon)+L_b\cos(\eta-\upsilon)]\vec{j} \\ &\quad +[l\cos(\theta-\upsilon)-L_b\sin(\eta-\upsilon)]\vec{k} \\ \vec{r}(t) &= [l(t)\sin(\theta(t)-\upsilon(t))+L_b\cos(\eta(t)-\upsilon(t))]\vec{j} \\ &\quad +[l(t)\cos(\theta(t)-\upsilon(t))-L_b\sin(\eta(t)-\upsilon(t))]\vec{k} \end{aligned} \tag{6}$$

where $\vec{j}$ and $\vec{k}$ are unit vectors along the Y_e and Z_e coordinate axes, respectively, $\vec{r}$ is a vector from the origin O of the NED coordinate frame to the payload, and $\vec{r}(t)$ is a vector function to describe the payload trajectory with respect to time. Additionally, it can be observed from the main control task that the payload swing angle in the NED coordinate frame needs to converge to zero, that is

$$\theta - \upsilon \to 0 \tag{7}$$

which can be deduced from the geometrical relationships of the ship-mounted crane system in Fig. 1. Hence, we can rearrange the desired payload position (y_d, z_d) in the NED coordinate frame as follows:

$$\begin{aligned} y_d &= L_b\cos(\eta_d-\upsilon) \\ z_d &= -L_b\sin(\eta_d-\upsilon)+l_d \\ \Longrightarrow \eta_d &= \upsilon+\arccos\left(\frac{y_d}{L_b}\right),\quad l_d = z_d-\sqrt{L_b^2-y_d^2} \end{aligned} \tag{8}$$

where η_d and l_d denote the desired boom pitch angle and rope length in the ship-fixed coordinate frame, respectively. It is not difficult to find that η_d is time-varying, which adds much difficulty to the controller design. To solve the aforementioned problem, we can merge the ship roll motion υ into the following new state variables:

$$\begin{aligned} &\xi_1 = \eta-\upsilon,\quad \xi_2 = l,\quad \xi_3 = \theta-\upsilon \\ \Longrightarrow &\boldsymbol{\xi} = [\xi_1 \quad \xi_2 \quad \xi_3]^\top. \end{aligned} \tag{9}$$

Consequently, the desired values of the new state variables ξ_1, ξ_2, ξ_3 are described as follows:

$$\xi_{1d} = \arccos\left(\frac{x_d}{L_b}\right),\quad \xi_{2d} = \sqrt{L_b^2-x_d^2}-y_d,\ \xi_{3d} = 0. \tag{10}$$

Then, the original ship-mounted crane systems' dynamics (1)–(3) can be rewritten as follows:

$$\begin{aligned} &\left(J+mL_b^2\right)\ddot{\xi}_1 - mL_bC_{1-3}\ddot{\xi}_2 - mL_bS_{1-3}\xi_2\ddot{\xi}_3 \\ &\quad -mL_bS_{1-3}\dot{\xi}_2\dot{\xi}_3 + mL_b(-S_{1-3}\dot{\xi}_2 + C_{1-3}\xi_2\dot{\xi}_3)\dot{\xi}_3 \\ &\quad +(mL_b+M_{ob})gC_1 = Z(u_1) \end{aligned} \tag{11}$$

$$\begin{aligned} &-mL_bC_{1-3}\ddot{\xi}_1 + m\ddot{\xi}_2 + mL_bS_{1-3}\dot{\xi}_1^2 - m\xi_2\dot{\xi}_3^2 \\ &\quad -mgC_3 = Z(u_2) \end{aligned} \tag{12}$$

$$\begin{aligned} &-mL_bS_{1-3}\xi_2\ddot{\xi}_1 + m\xi_2^2\ddot{\xi}_3 - mL_bC_{1-3}\xi_2\dot{\xi}_1^2 \\ &\quad +2m\xi_2\dot{\xi}_2\dot{\xi}_3 + mgS_3\xi_2 = -c\dot{\xi}_3. \end{aligned} \tag{13}$$

Combining (11) with (13) yields that

$$\begin{aligned} &\left(J+mL_b^2C_{1-3}^2\right)\ddot{\xi}_1 - mL_bC_{1-3}\ddot{\xi}_2 - mL_b^2S_{1-3}C_{1-3}\dot{\xi}_1^2 \\ &\quad +mgL_bS_{1-3}S_3 + cL_bS_{1-3}\frac{\dot{\xi}_3}{\xi_2} + mL_bC_{1-3}\xi_2\dot{\xi}_3^2 \\ &\quad +(mL_b+M_{ob})gC_1 = Z(u_1). \end{aligned} \tag{14}$$

Hence, we can rearrange the actuated dynamic equations (12) and (14) into a compact matrix-vector form as follows:

$$\ddot{\boldsymbol{\Xi}} = S(\boldsymbol{U}-\boldsymbol{T}) \tag{15}$$

where

$$\begin{aligned} S &= \begin{bmatrix} s_{11} & s_{12} \\ s_{21} & s_{22} \end{bmatrix} \\ \boldsymbol{\Xi} &= [\xi_1,\xi_2]^\top,\quad \boldsymbol{U} = [u_1,u_2]^\top,\ \boldsymbol{T} = [t_1,\ t_2]^\top \\ s_{11} &= \frac{1}{J},\quad s_{12} = s_{21} = \frac{L_bC_{1-3}}{J},\ s_{22} = \frac{mL_b^2C_{1-3}^2+J}{mJ} \\ t_1 &= -mL_b^2S_{1-3}C_{1-3}\dot{\xi}_1^2 + mgL_bS_{1-3}S_3 + cL_bS_{1-3}\frac{\dot{\xi}_3}{\xi_2} \\ &\quad +mL_bC_{1-3}\xi_2\dot{\xi}_3^2 + (mL_b+M_{ob})\,gC_1 - \Delta u_1 \\ t_2 &= mL_bS_{1-3}\dot{\xi}_1^2 - m\xi_2\dot{\xi}_3^2 - mgC_3 - \Delta u_2. \end{aligned} \tag{16}$$

Since the payload always swings beneath the boom tip in practical ship-mounted crane systems, we consider the following assumption, which has been widely utilized in the literature about cranes [1]–[22], [28]–[39], [42]–[44].

Assumption 1: The payload swing angle in the NED coordinate frame ξ_3 is bounded, and $|\xi_3| < \pi/2$.

In this paper, the major control task considered for ship-mounted crane systems consists of the following points:

1) to make the boom and rope travel to their desired positions in finite time and eliminate positioning errors;
2) to completely suppress payload residual swing in the NED coordinate frame;
3) to address the uncertain parameters/structures and nonlinear input dead zones.

III. Controller Design

In this section, we will provide the details of designing a control law to accomplish the above-mentioned control task. For clarity, the notations of necessary variables and parameters that will be involved in the controller design and analysis are listed in Table II.

First of all, S and $\boldsymbol{T}$ in (15) are considered as the unknown parts of ship-mounted crane dynamics, S_0 is the nominal value of S, and $S = \Delta S + S_0$. Hence, the above-mentioned dynamical equations in (15) can be rewritten as follows:

$$\begin{aligned} \ddot{\boldsymbol{\Xi}} &= S_0\boldsymbol{U} + \Delta S\boldsymbol{U} - S\boldsymbol{T} \\ &\triangleq S_0\boldsymbol{U} + \boldsymbol{B} \end{aligned} \tag{17}$$

TABLE II
VARIABLES AND PARAMETERS IN CONTROLLER DESIGN AND STABILITY ANALYSIS

Variables/parameters	Meaning	Variables/parameters	Meaning
$\xi_1,\ \xi_2,\ \xi_3$	to-be-controlled state variables	$\xi_{1d},\ \xi_{2d}$	desired values of $\xi_1,\ \xi_2$
$W_1,\ W_2$	output weight vectors	$V_1,\ V_2$	input weight matrices
$\hat{W}_1,\ \hat{W}_2$	estimates of $W_1,\ W_2$	$\hat{V}_1,\ \hat{V}_2$	estimates of $V_1,\ V_2$
$\tilde{W}_1,\ \tilde{W}_2$	estimation errors of $W_1,\ W_2$	$\tilde{V}_1,\ \tilde{V}_2$	estimation errors of $V_1,\ V_2$
$\epsilon_1,\ \epsilon_2$	approximation errors	$\bar{\epsilon}_1,\ \bar{\epsilon}_2$	upper bounds of $\epsilon_1,\ \epsilon_2$
$e_1,\ e_2$	positioning errors	$\phi_1,\ \phi_2$	sliding surfaces
$\sigma(\cdot)$	activation function	$\bar{\omega}_1,\ \bar{\omega}_2$	upper bounds of $\|\tilde{W}_1\|,\ \|\tilde{W}_2\|$
$\Omega_1,\ \Omega_2$	defined in (27)	$\Lambda_1,\ \Lambda_2$	defined in (28)
$\bar{\Lambda}_1,\ \bar{\Lambda}_2$	upper bounds of $\Lambda_1,\ \Lambda_2$	$\bar{\Omega}_1,\ \bar{\Omega}_2$	upper bounds of $\Omega_1,\ \Omega_2$
$k_{p1}, k_{p2}, k_1, k_2,$ $k_{v1}, k_{v2}, k_{\theta 1}, k_{\theta 2}$	control gains	$\alpha,\ \beta_1,\ \beta_2,$ $\gamma_1,\ \gamma_2$	positive parameters
$\Pi_1,\ \Pi_2,\ \Gamma_1,\ \Gamma_2$	positive diagonal parameter matrices		

where $\boldsymbol{B}$ can be approximated by the following double-layer neural network structures[1]:

$$\boldsymbol{B} = \left[W_1^\top \sigma\left(V_1^\top \boldsymbol{x}\right) + \epsilon_1, W_2^\top \sigma\left(V_2^\top \boldsymbol{x}\right) + \epsilon_2\right]^\top \tag{18}$$

where $\boldsymbol{x} = [\xi_1, \xi_2, \xi_3, \dot{\xi}_1, \dot{\xi}_2, \dot{\xi}_3, 1]^\top$, $\sigma(\cdot)$ is an activation function, V_1 and V_2 are bounded input weight matrices, W_1 and W_2 are bounded output weight vectors [50], and ϵ_1 and ϵ_2 are approximation errors with the upper bounds $\bar{\epsilon}_1$ and $\bar{\epsilon}_2$, respectively.[2]

Next, the positioning errors of the boom and rope, e_1 and e_2, are defined as

$$e_1 = \xi_1 - \xi_{1d}, \quad e_2 = \xi_2 - \xi_{2d}. \tag{19}$$

Furthermore, a sliding manifold $\boldsymbol{\Phi} = [\varphi_1, \varphi_2]^\top$ related to e_1 and e_2 is constructed as follows:

$$\begin{aligned} &\varphi_1 = k_1 e_1 + \dot{e}_1, \quad \varphi_2 = k_2 e_2 + \dot{e}_2 \\ \Longrightarrow\ &\dot{\varphi}_1 = k_1 \dot{e}_1 + \ddot{e}_1 = k_1 \dot{e}_1 + \ddot{\xi}_1 - \ddot{\xi}_{1d} \\ &\dot{\varphi}_2 = k_2 \dot{e}_2 + \ddot{e}_2 = k_2 \dot{e}_2 + \ddot{\xi}_2 - \ddot{\xi}_{2d} \end{aligned} \tag{20}$$

where k_1 and k_2 are positive parameters. Then, by differentiating $\boldsymbol{\Phi}$ with respect to time, one can obtain the following result:

$$\begin{bmatrix} \dot{\varphi}_1 \\ \dot{\varphi}_2 \end{bmatrix} = S_0 \begin{bmatrix} u_1 \\ u_2 \end{bmatrix} + \begin{bmatrix} W_1^\top \sigma\left(V_1^\top \boldsymbol{x}\right) + \epsilon_1 \\ W_2^\top \sigma\left(V_2^\top \boldsymbol{x}\right) + \epsilon_2 \end{bmatrix} + \begin{bmatrix} k_1 \dot{e}_1 \\ k_2 \dot{e}_2 \end{bmatrix} - \begin{bmatrix} \ddot{\xi}_{1d} \\ \ddot{\xi}_{2d} \end{bmatrix}. \tag{21}$$

Hence, we design the following nonlinear neural network-based control law:

$$\begin{bmatrix} u_1 \\ u_2 \end{bmatrix} = S_0^{-1} \begin{bmatrix} -\hat{W}_1^\top \sigma\left(\hat{V}_1^\top \boldsymbol{x}\right) - \Delta_1 \\ -\hat{W}_2^\top \sigma\left(\hat{V}_2^\top \boldsymbol{x}\right) - \Delta_2 \end{bmatrix} \tag{22}$$

where $\hat{W}_1$, $\hat{W}_2$, $\hat{V}_1$, and $\hat{V}_2$ are the corresponding estimates of W_1, W_2, V_1, and V_2, respectively, and

$$\begin{aligned} \Delta_1 &= k_1 \dot{e}_1 - \ddot{\xi}_{1d} + k_{p1}\varphi_1 + k_{v1}\text{sign}(\varphi_1) \\ &\quad + k_{\theta 1}(1 - \cos\xi_3)\xi_3^2 \varphi_1 \\ \Delta_2 &= k_2 \dot{e}_2 - \ddot{\xi}_{2d} + k_{p2}\varphi_2 + k_{v2}\text{sign}(\varphi_2) \\ &\quad + k_{\theta 2}(1 - \cos\xi_3)\xi_3^2 \varphi_2 \\ \sigma(z) &= \frac{1}{1 + e^{-z}} \end{aligned} \tag{23}$$

where $\sigma(\cdot)$ and its derivative $\dot{\sigma}(\cdot)$ are both bounded. The last terms in Δ_1 and Δ_2 are introduced to increase the coupling relationship of the state variables and further improve the antiswing performance. Moreover, k_{p1}, k_{p2}, k_{v1}, k_{v2}, $k_{\theta 1}$, and $k_{\theta 2}$ are positive gains to be determined, which need to meet the following conditions *theoretically* based on the subsequent Lyapunov-based stability analysis:

$$\begin{aligned} &k_{p1}, k_{p2}, k_{\theta 1}, k_{\theta 2} > 0, \\ &\qquad k_{v1} > \max\{\bar{\Lambda}_1, \bar{\Omega}_1\}, \quad k_{v2} > \max\{\bar{\Lambda}_2, \bar{\Omega}_2\} \end{aligned} \tag{24}$$

where $\bar{\Lambda}_1$, $\bar{\Lambda}_2$, $\bar{\Omega}_1$, and $\bar{\Omega}_2$ will be defined subsequently.

By substituting (22) into (21), it is easy to derive that

$$\begin{aligned} \dot{\varphi}_1 &= W_1^\top \sigma\left(V_1^\top \boldsymbol{x}\right) - \hat{W}_1^\top \sigma\left(\hat{V}_1^\top \boldsymbol{x}\right) + \epsilon_1 - k_{p1}\varphi_1 \\ &\quad - k_{v1}\text{sign}(\varphi_1) - k_{\theta 1}(1 - \cos\xi_3)\xi_3^2 \varphi_1 \\ \dot{\varphi}_2 &= W_2^\top \sigma\left(V_2^\top \boldsymbol{x}\right) - \hat{W}_2^\top \sigma\left(\hat{V}_2^\top \boldsymbol{x}\right) + \epsilon_2 - k_{p2}\varphi_2 \\ &\quad - k_{v2}\text{sign}(\varphi_2) - k_{\theta 2}(1 - \cos\xi_3)\xi_3^2 \varphi_2. \end{aligned} \tag{25}$$

Next, we define the estimation errors $\tilde{W}_1$, $\tilde{W}_2$, $\tilde{V}_1$, and $\tilde{V}_2$ as

$$\begin{aligned} &\tilde{W}_1 = W_1 - \hat{W}_1, \quad \tilde{W}_2 = W_2 - \hat{W}_2 \\ &\tilde{V}_1 = V_1 - \hat{V}_1, \quad \tilde{V}_2 = V_2 - \hat{V}_2. \end{aligned} \tag{26}$$

In order to facilitate the subsequent stability analysis, we first define the following compact set B_w:

$$B_w = \left\{\tilde{W}_1 \in \Re^N, \tilde{W}_2 \in \Re^N :\ \|\tilde{W}_1\| \le \bar{\omega}_1, \|\tilde{W}_2\| \le \bar{\omega}_2\right\}$$

where N is the number of neurons and $\bar{\omega}_1$ and $\bar{\omega}_2$ are the radii of the ellipsoid B_w. Furthermore, after some strict mathematical calculations, we can rearrange the first three terms of $\dot{\varphi}_1$ and $\dot{\varphi}_2$ as the following forms (the corresponding

[1]The last constant term in $\boldsymbol{x}$ is introduced to increase the flexibility of the double-layer neural network, which can generate the bias terms and make the network better approximate the system unknown parts.

[2]Owing to the inherent property of neural networks, the neural network approximation errors ϵ_1 and ϵ_2 always exist and have the upper bounds $\bar{\epsilon}_1$ and $\bar{\epsilon}_2$, respectively, which is a widely used assumption in neural network-related studies (see [48]–[50]). Moreover, $\bar{\epsilon}_1$ and $\bar{\epsilon}_2$ will not be influenced by the state variables during the entire analysis process.

derivations are shown in the Appendix):

$$\begin{aligned}\Omega_1 &\triangleq W_1^\top \sigma\left(V_1^\top \boldsymbol{x}\right) - \hat{W}_1^\top \sigma\left(\hat{V}_1^\top \boldsymbol{x}\right) + \epsilon_1 \\ &= \tilde{W}_1^\top \sigma\left(\hat{V}_1^\top \boldsymbol{x}\right) - \tilde{W}_1^\top \dot{\sigma}\left(\hat{V}_1^\top \boldsymbol{x}\right)\hat{V}_1^\top \boldsymbol{x} \\ &\quad + \hat{W}_1^\top \dot{\sigma}\left(\hat{V}_1^\top \boldsymbol{x}\right)\tilde{V}_1^\top \boldsymbol{x} + \Lambda_1 \\ \Omega_2 &\triangleq W_2^\top \sigma\left(V_2^\top \boldsymbol{x}\right) - \hat{W}_2^\top \sigma\left(\hat{V}_2^\top \boldsymbol{x}\right) + \epsilon_2 \\ &= \tilde{W}_2^\top \sigma\left(\hat{V}_2^\top \boldsymbol{x}\right) - \tilde{W}_2^\top \dot{\sigma}\left(\hat{V}_2^\top \boldsymbol{x}\right)\hat{V}_2^\top \boldsymbol{x} \\ &\quad + \hat{W}_2^\top \dot{\sigma}\left(\hat{V}_2^\top \boldsymbol{x}\right)\tilde{V}_2^\top \boldsymbol{x} + \Lambda_2 \end{aligned} \tag{27}$$

where

$$\begin{aligned}\Lambda_1 &= \tilde{W}_1^\top \dot{\sigma}\left(\hat{V}_1^\top \boldsymbol{x}\right)V_1^\top \boldsymbol{x} + W_1^\top O\left(\tilde{V}_1^\top \boldsymbol{x}\right)^2 + \epsilon_1 \\ \Lambda_2 &= \tilde{W}_2^\top \dot{\sigma}\left(\hat{V}_2^\top \boldsymbol{x}\right)V_2^\top \boldsymbol{x} + W_2^\top O\left(\tilde{V}_2^\top \boldsymbol{x}\right)^2 + \epsilon_2. \end{aligned} \tag{28}$$

Moreover, for the given compact set B_w, the functions Λ_1 and Λ_2 have upper bounds as

$$\Lambda_1 \le \bar{\Lambda}_1, \Lambda_2 \le \bar{\Lambda}_2. \tag{29}$$

The update laws of $\hat{W}_1$, $\hat{W}_2$, $\hat{V}_1$, and $\hat{V}_2$ are designed as follows:

$$\begin{aligned}\dot{\hat{W}}_1 &= \beta_1 \alpha \varphi_1 \Pi_1\left[\sigma\left(\hat{V}_1^\top \boldsymbol{x}\right) - \dot{\sigma}\left(\hat{V}_1^\top \boldsymbol{x}\right)\hat{V}_1^\top \boldsymbol{x}\right] \\ \dot{\hat{W}}_2 &= \beta_2 \alpha \varphi_2 \Pi_2\left[\sigma\left(\hat{V}_2^\top \boldsymbol{x}\right) - \dot{\sigma}\left(\hat{V}_2^\top \boldsymbol{x}\right)\hat{V}_2^\top \boldsymbol{x}\right] \\ \dot{\hat{V}}_1 &= \gamma_1 \alpha \varphi_1 \Gamma_1 \boldsymbol{x}\hat{W}_1^\top \dot{\sigma}\left(\hat{V}_1^\top \boldsymbol{x}\right) \\ \dot{\hat{V}}_2 &= \gamma_2 \alpha \varphi_2 \Gamma_2 \boldsymbol{x}\hat{W}_2^\top \dot{\sigma}\left(\hat{V}_2^\top \boldsymbol{x}\right) \end{aligned} \tag{30}$$

where $\alpha, \beta_1, \beta_2, \gamma_1$, and γ_2 are positive parameters and Π_1, Π_2, Γ_1, and Γ_2 are positive diagonal parameter matrices.

Remark 1: Neural network structures are a kind of useful tool to approximate unknown parts of systems and improve robustness [50]–[52]. Hence, some neural network-based controllers can be employed in *fully actuated* systems to achieve adaptive control. However, as far as we know, in most cases, only *partial* state variables can be effectively controlled when they are applied to *underactuated* systems. In this paper, after strict theoretical analysis, not only the *actuated* state variables (i.e., the boom pitch angle and the rope length) but also the *unactuated* state variable (i.e., the payload swing angle) can converge to their desired values and keep stable by means of the presented nonlinear control method, as stated in Theorem 1.

Remark 2: In fact, B_w denotes a given compact set, whose validity will be proven in (31)–(35), rather than a conclusion or a default assumption. Moreover, in the compact set B_w, the functions Λ_1 and Λ_2 are composed of bounded variables, bounded functions, and high-order infinitesimal terms (hence bounded); as a result, there also exist upper bounds $\bar{\Lambda}_1$ and $\bar{\Lambda}_2$ for Λ_1 and Λ_2, respectively. It is worth pointing out that after a series of stability analysis in Section IV, we can prove that $\|\tilde{W}_1\| \le \bar{\omega}_1$ and $\|\tilde{W}_2\| \le \bar{\omega}_2$ are always valid; hence, Λ_1 and Λ_2 are also always bounded for $\forall\ t \ge 0$.

Remark 3: It is noted that the unknown/uncertain dead-zone functions $\triangle u_1$ and $\triangle u_2$ will not make t_1 and t_2 unbounded. In particular, after the strict stability analysis in Section IV, we can conclude that for the proposed control approach, the state variables and weight estimates included in u_1 and u_2 can converge to their desired values and keep bounded for $\forall\ t \ge 0$, respectively. In other words, u_1 and u_2 will not tend to infinity during the entire control process, as shown in (34). Hence, the double-layer neural network can estimate the unknown nonlinear functions of actuator dead zones.

IV. Stability/Convergence Analysis

In this section, we will theoretically implement the strict stability analysis for the proposed controller.

Theorem 1: For underactuated ship-mounted cranes suffering from ship roll motions and input dead-zone effects, by means of the presented controller (22) and the update law (30), the actuated boom and rope can reach their desired positions in finite time, and moreover, the payload swing angle is also damped to zero, that is

$$\begin{aligned}\lim_{t\to t_f}[\xi_1, \dot{\xi}_1, \ddot{\xi}_1]^\top &= [\xi_{1d}, 0, 0]^\top \\ \lim_{t\to t_f}[\xi_2, \dot{\xi}_2, \ddot{\xi}_2]^\top &= [\xi_{2d}, 0, 0]^\top \\ \lim_{t\to \infty}[\xi_3, \dot{\xi}_3, \ddot{\xi}_3]^\top &= [0, 0, 0]^\top \end{aligned}$$

where t_f is a finite time.

Proof: To prove Theorem 1, we first construct the following Lyapunov function candidate $H_1(t)$:

$$\begin{aligned}H_1 = \frac{\alpha}{2}\boldsymbol{\Phi}^\top \boldsymbol{\Phi} &+ \frac{1}{2\gamma_1}\mathrm{Tr}\left(\tilde{V}_1^\top \Gamma^{-1}\tilde{V}_1\right) + \frac{1}{2\gamma_2}\mathrm{Tr}\left(\tilde{V}_2^\top \Gamma^{-1}\tilde{V}_2\right) \\ &+ \frac{1}{2\beta_1}\tilde{W}_1^\top \Pi^{-1}\tilde{W}_1 + \frac{1}{2\beta_2}\tilde{W}_2^\top \Pi^{-1}\tilde{W}_2. \end{aligned} \tag{31}$$

Then, together with (25) and (27), we can differentiate (31) with respect to time to obtain $\dot{H}_1(t)$ as follows:

$$\begin{aligned}\dot{H}_1 &= \alpha \boldsymbol{\Phi}^\top \dot{\boldsymbol{\Phi}} + \frac{1}{\gamma_1}\mathrm{Tr}\left(\tilde{V}_1^\top \Gamma^{-1}\dot{\tilde{V}}_1\right) + \frac{1}{\gamma_2}\mathrm{Tr}\left(\tilde{V}_2^\top \Gamma^{-1}\dot{\tilde{V}}_2\right) \\ &\quad + \frac{1}{\beta_1}\tilde{W}_1^\top \Pi^{-1}\dot{\tilde{W}}_1 + \frac{1}{\beta_2}\tilde{W}_2^\top \Pi^{-1}\dot{\tilde{W}}_2 \\ &= \alpha\varphi_1\left[\tilde{W}_1^\top \sigma\left(\hat{V}_1^\top \boldsymbol{x}\right) - \tilde{W}_1^\top \dot{\sigma}\left(\hat{V}_1^\top \boldsymbol{x}\right)\hat{V}_1^\top \boldsymbol{x}\right. \\ &\qquad \left. + \hat{W}_1^\top \dot{\sigma}\left(\hat{V}_1^\top \boldsymbol{x}\right)\tilde{V}_1^\top \boldsymbol{x}\right] + \alpha\varphi_1\Lambda_1 - \alpha k_{\theta 1}(1-\cos\xi_3) \\ &\quad \cdot \xi_3^2\varphi_1^2 - \alpha k_{p1}\varphi_1^2 - \alpha k_{v1}|\varphi_1| - \alpha k_{p2}\varphi_2^2 - \alpha k_{v2}|\varphi_2| \\ &\quad + \alpha\varphi_2\left[\tilde{W}_2^\top \sigma\left(\hat{V}_2^\top \boldsymbol{x}\right) - \tilde{W}_2^\top \dot{\sigma}\left(\hat{V}_2^\top \boldsymbol{x}\right)\hat{V}_2^\top \boldsymbol{x}\right. \\ &\qquad \left. + \hat{W}_2^\top \dot{\sigma}\left(\hat{V}_2^\top \boldsymbol{x}\right)\tilde{V}_2^\top \boldsymbol{x}\right] + \alpha\varphi_2\Lambda_2 \\ &\quad - \alpha k_{\theta 2}(1-\cos\xi_3) \\ &\quad \cdot \xi_3^2\varphi_2^2 - \frac{1}{\gamma_1}\mathrm{Tr}\left[\tilde{V}_1^\top \Gamma_1^{-1}\gamma_1\alpha\varphi_1\Gamma_1 \boldsymbol{x}\hat{W}_1^\top \dot{\sigma}\left(\hat{V}_1^\top \boldsymbol{x}\right)\right] \\ &\quad - \frac{1}{\gamma_2}\mathrm{Tr}\left[\tilde{V}_2^\top \Gamma_2^{-1}\gamma_2\alpha\varphi_2\Gamma_2 \boldsymbol{x}\hat{W}_2^\top \dot{\sigma}\left(\hat{V}_2^\top \boldsymbol{x}\right)\right] \\ &\quad - \frac{1}{\beta_1}\tilde{W}_1^\top \Pi_1^{-1}\left[\beta_1\alpha\varphi_1\Pi_1\left(\sigma\left(\hat{V}_1^\top \boldsymbol{x}\right)\right.\right. \\ &\quad \left.\left. - \dot{\sigma}\left(\hat{V}_1^\top \boldsymbol{x}\right)\hat{V}_1^\top \boldsymbol{x}\right)\right] - \frac{1}{\beta_2}\tilde{W}_2^\top \Pi_2^{-1} \\ &\quad \cdot \left[\beta_2\alpha\varphi_2\Pi_2\left(\sigma\left(\hat{V}_2^\top \boldsymbol{x}\right) - \dot{\sigma}\left(\hat{V}_2^\top \boldsymbol{x}\right)\hat{V}_2^\top \boldsymbol{x}\right)\right] \\ &= -\alpha k_{p1}\varphi_1^2 - \alpha k_{v1}|\varphi_1| - \alpha k_{p2}\varphi_2^2 - \alpha k_{v2}|\varphi_2| \\ &\quad - \alpha k_{\theta 1}(1-\cos\xi_3)\xi_3^2\varphi_1^2 - \alpha k_{\theta 2}(1-\cos\xi_3)\xi_3^2\varphi_2^2 \\ &\quad + \alpha\varphi_1\Lambda_1 + \alpha\varphi_2\Lambda_2. \end{aligned} \tag{32}$$

Considering the fact of $\Lambda_1 \le \bar{\Lambda}_1$ and $\Lambda_2 \le \bar{\Lambda}_2$ [see (29)], it can be found that

$$\begin{aligned}\dot{H}_1 &\le -\alpha k_{p1}\varphi_1^2 - \alpha k_{v1}|\varphi_1| - \alpha k_{p2}\varphi_2^2 - \alpha k_{v2}|\varphi_2| \\ &\quad + \alpha|\varphi_1|\bar{\Lambda}_1 + \alpha|\varphi_2|\bar{\Lambda}_2 \\ &= -\alpha(k_{v1} - \bar{\Lambda}_1)|\varphi_1| - \alpha(k_{v2} - \bar{\Lambda}_2)|\varphi_2| \\ &\quad - \alpha k_{p1}\varphi_1^2 - \alpha k_{p2}\varphi_2^2. \end{aligned} \tag{33}$$

Hence, when the initial values of the weight estimation errors are set within the compact set B_w and when the control gains k_{v1} and k_{v2} satisfy the conditions in (24), we can obtain that

$$\begin{aligned}\dot{H}_1 \le 0 &\Longrightarrow H_1 \in \mathcal{L}_\infty \\ &\Longrightarrow \tilde{W}_1, \tilde{W}_2, \tilde{V}_1, \tilde{V}_2 \in \mathcal{L}_\infty \\ &\Longrightarrow u_1, u_2 \in \mathcal{L}_\infty \end{aligned} \tag{34}$$

and

$$\lim_{t\to\infty} \boldsymbol{\Phi} = [\varphi_1, \varphi_2]^\top = [0, 0]^\top. \tag{35}$$

As a result, the equilibrium point of actuated variables in ship-mounted crane systems is asymptotically stable. Moreover, the weight estimation errors included in $H_1(t)$, i.e., $\tilde{W}_1, \tilde{W}_2, \tilde{V}_1$, and $\tilde{V}_2$, remain bounded for $\forall\ t \ge 0$ and $\|\tilde{W}_1\|$ and $\|\tilde{W}_2\|$ can always be limited within the range of $\bar{\omega}_1$ and $\bar{\omega}_2$, respectively. However, based on the above-mentioned analysis, it is difficult to guarantee the sliding manifold $\boldsymbol{\Phi}$ to converge to zero in finite time. Hence, we further present a modified Lyapunov function candidate $H_2(t)$ as follows:

$$H_2 = \frac{\alpha}{2}\boldsymbol{\Phi}^\top\boldsymbol{\Phi}. \tag{36}$$

Based on the results of (34), one can conclude that $\tilde{V}_1, \tilde{V}_2, \hat{V}_1$, and $\hat{V}_2$ in (27) are bounded, which indicates that

$$\begin{aligned}\Omega_1 &= W_1^\top\sigma\left(V_1^\top\boldsymbol{x}\right) - \hat{W}_1^\top\sigma\left(\hat{V}_1^\top\boldsymbol{x}\right) + \epsilon_1 \le \bar{\Omega}_1 \\ \Omega_2 &= W_2^\top\sigma\left(V_2^\top\boldsymbol{x}\right) - \hat{W}_2^\top\sigma\left(\hat{V}_2^\top\boldsymbol{x}\right) + \epsilon_2 \le \bar{\Omega}_2 \end{aligned} \tag{37}$$

where $\bar{\Omega}_1$ and $\bar{\Omega}_2$ are positive upper bounds of Ω_1 and Ω_2, respectively. Hence, by differentiating (36), $\dot{H}_2(t)$ can be expressed as

$$\begin{aligned}\dot{H}_2 &\le -\alpha k_{p1}\varphi_1^2 - \alpha k_{v1}|\varphi_1| - \alpha k_{p2}\varphi_2^2 - \alpha k_{v2}|\varphi_2| \\ &\quad + \alpha|\varphi_1|\bar{\Omega}_1 + \alpha|\varphi_2|\bar{\Omega}_2 \\ &= -\alpha(k_{v1} - \bar{\Omega}_1)|\varphi_1| - \alpha(k_{v2} - \bar{\Omega}_2)|\varphi_2| \\ &\quad - \alpha k_{p1}\varphi_1^2 - \alpha k_{p2}\varphi_2^2 \\ &\le -\alpha(k_{v1} - \bar{\Omega}_1)|\varphi_1| - \alpha(k_{v2} - \bar{\Omega}_2)|\varphi_2| \\ &\le -\kappa\|\boldsymbol{\Phi}\| \le 0 \end{aligned} \tag{38}$$

where $\kappa \triangleq \min\{\alpha(k_{v1} - \bar{\Omega}_1), \alpha(k_{v2} - \bar{\Omega}_2)\}$. Consequently, we can obtain the following conclusion:

$$\begin{aligned}\dot{H}_2 &\le -\frac{\kappa}{\alpha}\sqrt{2\alpha H_2} \\ \Longrightarrow \sqrt{H_2(t)} - \sqrt{H_2(0)} &\le -\frac{\kappa}{\sqrt{2\alpha}}t. \end{aligned} \tag{39}$$

Assume that the state variables will converge to the sliding surface $\boldsymbol{\Phi} = [\varphi_1, \varphi_2]^\top$ at the time t_f, i.e., $H_2(t_f) = 0$. Then, (39) can be rewritten as

$$t_f \le \frac{\sqrt{2\alpha}}{\kappa}\sqrt{H_2(0)} \tag{40}$$

which means that the convergence time t_f of the sliding surface $\boldsymbol{\Phi}$ is finite, and moreover, owing to $\dot{H}_2(t) \le 0$, it is obvious that

$$\begin{aligned}&0 \le H_2(t) \le H_2(t_f) = 0 \quad \forall t \ge t_f \\ \Longrightarrow\ &H_2(t) = 0 \quad \forall t \ge t_f \\ \Longrightarrow\ &\boldsymbol{\Phi} = [\varphi_1, \varphi_2]^\top = [0, 0]^\top \quad \forall t \ge t_f. \end{aligned} \tag{41}$$

Consequently, the sliding surface $\boldsymbol{\Phi}$ is an invariant set after t_f, that is

$$\dot{\boldsymbol{\Phi}} = [\dot{\varphi}_1, \dot{\varphi}_2]^\top = [0, 0]^\top \quad \forall t \ge t_f. \tag{42}$$

Next, we will theoretically analyze the convergence of the payload swing angle. First, together with (20), one can rearrange (13) as follows:

$$\begin{aligned}\ddot{\xi}_3 &= -\frac{gS_3}{\xi_2} - \left(\frac{c}{m\xi_2^2} + \frac{2\dot{\xi}_2}{\xi_2}\right)\dot{\xi}_3 + \frac{L_b}{\xi_2}\left(C_{1-3}\dot{\xi}_1^2 + S_{1-3}\ddot{\xi}_1\right) \\ &= -\frac{gS_3}{\xi_2} - \left(\frac{c}{m\xi_2^2} + \frac{2\dot{\xi}_2}{\xi_2}\right)\dot{\xi}_3 \\ &\quad + \frac{L_b}{\xi_2}\left[C_{1-3}\dot{\xi}_1^2 + S_{1-3}\cdot(\dot{\varphi}_1 + \ddot{\xi}_{1d} - k_1\dot{e}_1)\right]. \end{aligned} \tag{43}$$

Second, we construct a Lyapunov function candidate $H_3(t)$ as follows:

$$H_3 = \frac{1}{2}\xi_2\dot{\xi}_3^2 + g(1 - \cos\xi_3). \tag{44}$$

Then, by taking the time derivative of $H_3(t)$ and substituting (43) into $\dot{H}_3(t)$, we can obtain that

$$\begin{aligned}\dot{H}_3 &= \xi_2\dot{\xi}_3\ddot{\xi}_3 + \frac{1}{2}\dot{\xi}_2\dot{\xi}_3^2 + g\sin\xi_3\dot{\xi}_3 \\ &= -\left(\frac{c}{m\xi_2} + \frac{3}{2}\dot{\xi}_2\right)\dot{\xi}_3^2 \\ &\quad + L_b\left[C_{1-3}\dot{\xi}_1^2 + S_{1-3}\cdot(\dot{\varphi}_1 + \ddot{\xi}_{1d} - k_1\dot{e}_1)\right]\dot{\xi}_3 \\ &= -\chi\dot{\xi}_3^2 + \Psi\dot{\xi}_3 \end{aligned} \tag{45}$$

where

$$\begin{aligned}\chi &\triangleq \frac{c}{m\xi_2} + \frac{3}{2}\dot{\xi}_2 \\ \Psi &\triangleq L_b\left[C_{1-3}\dot{\xi}_1^2 + S_{1-3}(\dot{\varphi}_1 + \ddot{\xi}_{1d} - k_1\dot{e}_1)\right]. \end{aligned} \tag{46}$$

It can be seen from (45) that $\dot{H}_3$ is negative, i.e., $H_3 \in \mathcal{L}_\infty$, in the case of $|\dot{\xi}_3| > |\Psi|/|\chi|$, which implies that $\dot{\xi}_3 \in \mathcal{L}_\infty$. Then, together with (41)–(43), we can find that

$$\dot{\xi}_3 \in \mathcal{L}_\infty \Longrightarrow \ddot{\xi}_3 \in \mathcal{L}_\infty. \tag{47}$$

Next, we regard the third term on the right-hand side of (43) as a virtual control input u_v, that is

$$u_v = \frac{L_b}{\xi_2}\left[C_{1-3}\dot{\xi}_1^2 + S_{1-3}(\dot{\varphi}_1 + \ddot{\xi}_{1d} - k_1\dot{e}_1)\right]$$

and then independently consider the following "zero-input" dynamic equation ($u_v = 0$):

$$\ddot{\xi}_3 = -\frac{gS_3}{\xi_2} - \left(\frac{c}{m\xi_2^2} + \frac{2\dot{\xi}_2}{\xi_2}\right)\dot{\xi}_3 \tag{48}$$

$$\Longrightarrow \dot{H}_3 = -\left(\frac{c}{m\xi_2} + \frac{3}{2}\dot{\xi}_2\right)\dot{\xi}_3^2 = -\chi\dot{\xi}_3^2. \tag{49}$$

Thus, the integral of (49) with respect to time can be expressed as

$$H_3(0) - H_3(\infty) = \int_0^\infty \left(\frac{c}{m\xi_2} + \frac{3}{2}\dot{\xi}_2\right)\dot{\xi}_3^2 dt = \int_0^\infty \frac{c}{m\xi_2}\dot{\xi}_3^2 dt + \frac{3}{2}\int_0^\infty \dot{\xi}_2\dot{\xi}_3^2 dt.$$

Considering the fact of

$$\left(\xi_2\dot{\xi}_3^2\right)' = \dot{\xi}_2\dot{\xi}_3^2 + 2\xi_2\dot{\xi}_3\ddot{\xi}_3$$

where $(\xi_2\dot{\xi}_3^2)'$ denotes the derivative of $\xi_2\dot{\xi}_3^2$ with respect to time, it is clear that

$$H_3(0) - H_3(\infty) = \int_0^\infty \frac{c}{m\xi_2}\dot{\xi}_3^2 dt + \frac{3}{2}\int_0^\infty \left(\xi_2\dot{\xi}_3^2\right)' dt - 3\int_0^\infty \xi_2\dot{\xi}_3\ddot{\xi}_3 dt. \quad (50)$$

Moreover, due to $\xi_2 = \xi_{2d}$, $\forall t \geq t_f$ [see (41)], we can carry out the following calculation:

$$\begin{aligned}\int_0^\infty \xi_2\dot{\xi}_3\ddot{\xi}_3 dt &= \int_0^{\dot{\xi}_3(t_f)} \xi_2\dot{\xi}_3 d\dot{\xi}_3 + \xi_{2d}\int_{\dot{\xi}_3(t_f)}^{\dot{\xi}_3(\infty)} \dot{\xi}_3 d\dot{\xi}_3 \\ &= \int_0^{\dot{\xi}_3(t_f)} \xi_2\dot{\xi}_3 d\dot{\xi}_3 + \frac{1}{2}\xi_{2d}\left[\dot{\xi}_3^2(\infty) - \dot{\xi}_3^2(t_f)\right]. \quad (51)\end{aligned}$$

Due to $\dot{\xi}_3 \in \mathcal{L}_\infty$ and $\xi_2 \in \mathcal{L}_\infty$, it is not difficult to find that

$$\begin{aligned}&\frac{3}{2}\int_0^\infty \left(\xi_2\dot{\xi}_3^2\right)' dt = \frac{3}{2}\xi_2\dot{\xi}_3^2 \in \mathcal{L}_\infty \\ &\int_0^{\dot{\xi}_3(t_f)} \xi_2\dot{\xi}_3\, d\dot{\xi}_3 \in \mathcal{L}_\infty, \quad \frac{1}{2}\xi_{2d}\left[\dot{\xi}_3^2(\infty) - \dot{\xi}_3^2(t_f)\right] \in \mathcal{L}_\infty \\ \Longrightarrow &\int_0^\infty \xi_2\dot{\xi}_3\ddot{\xi}_3\, dt \in \mathcal{L}_\infty. \quad (52)\end{aligned}$$

As a result, (50) can be rearranged as

$$\int_0^\infty \frac{c}{m\xi_2}\dot{\xi}_3^2\, dt = H_3(0) - H_3(\infty) - \frac{3}{2}\xi_2\dot{\xi}_3^2 + 3\int_0^\infty \xi_2\dot{\xi}_3\ddot{\xi}_3\, dt \in \mathcal{L}_\infty$$

which means that

$$\frac{c}{m\bar{l}}\int_0^\infty \dot{\xi}_3^2\, dt \leq \int_0^\infty \frac{c}{m\xi_2}\dot{\xi}_3^2\, dt \in \mathcal{L}_\infty \Longrightarrow \dot{\xi}_3 \in \mathcal{L}_2. \quad (53)$$

In accordance with Barbalat's lemma [53], based on (47) and (53), it is easy to obtain the following conclusion:

$$\lim_{t\to\infty} \dot{\xi}_3 = 0. \quad (54)$$

Additionally, considering the fact of

$$\left(\frac{gS_3}{\xi_2}\right)' \in \mathcal{L}_\infty \quad (55)$$

one can conclude that

$$\lim_{t\to\infty} \ddot{\xi}_3 = 0, \quad \lim_{t\to\infty} \sin\xi_3 = 0 \Longrightarrow \lim_{t\to\infty} \xi_3 = 0 \quad (56)$$

where the extended Barbalat's lemma [53] and Assumption 1 are used. Hence, the equilibrium point of the "zero-input" dynamic system in (48) is asymptotically stable. Then, combining (41) and (42) yields that

$$\lim_{t\to\infty} \frac{L_b}{\xi_2}\left[C_{1-3}\dot{\xi}_1^2 + S_{1-3}(\dot{\varphi}_1 + \ddot{\xi}_{1d} - k_1\dot{e}_1)\right] = 0. \quad (57)$$

Moreover, due to the fact of $\dot{\xi}_3 \in \mathcal{L}_\infty$, $\forall t \geq 0$, the unactuated dynamic model (43) satisfies the property of CIBS in [54]. Hence, based on (57) and the conclusion that (48) is an asymptotically stable system, it can be found from the theorem in [54] that for the entire unactuated dynamics (43)

$$\lim_{t\to\infty} \dot{\xi}_3 = 0. \quad (58)$$

Similarly, by utilizing the extended Barbalat's lemma [53], one can obtain the following result from (55) and (57):

$$\lim_{t\to\infty} \xi_3 = \ddot{\xi}_3 = 0. \quad (59)$$

Hence, the payload swing angle is asymptotically convergent. In summary, by combining the conclusions in (41), (42), (58), and (59), the entire proof of Theorem 1 is accomplished. ■

Remark 4: Based on the analysis in Theorem 1, it is found that the state variables of ship-mounted crane systems are always bounded, as shown in (41), (42), (58), and (59); as a result, the boundedness of the system unknown parts can be theoretically guaranteed. Additionally, in this paper, the fact of $\|\tilde{W}_1\| \leq \bar{\omega}_1$ and $\|\tilde{W}_2\| \leq \bar{\omega}_2$ is always valid, i.e., it can be theoretically proven that the weight estimation errors can always be limited within the compact set B_w. Hence, during the controller design and stability analysis, the compact set B_w does not change along with the variation of the bounded state variables theoretically.

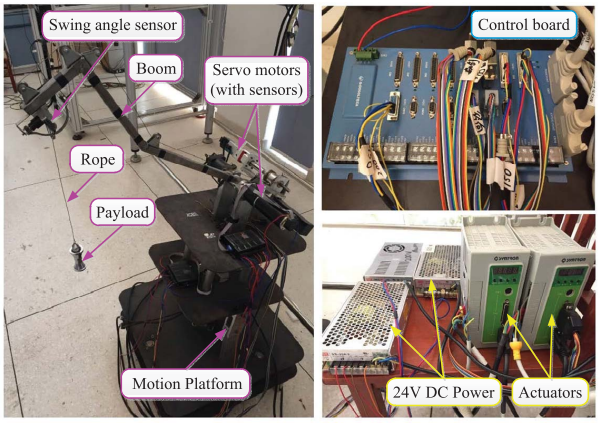

Fig. 3. Self-built ship-mounted crane experiment platform.

V. Experimental Results

In this section, we will validate the feasibility and robustness of the proposed controller by comparing it with the existing approaches, changing plant parameters, adding external unknown/uncertain disturbances, and considering irregular wave-induced ship motions.

The self-built ship-mounted crane experimental platform (see Fig. 3) consists of the core control part (including the host computer and control board), the driving part (including the

servo actuators and 24-V power supply), and the mechanical structure (mainly composed of a boom and a payload connected with a rope). Apart from that, two separate servo motors control the boom pitch movement and the rope length, respectively, and the other one at the bottom of the platform can imitate the ship roll motions induced by sea waves. Moreover, the boom pitch angle, the rope length, and the payload swing angle, which are considered as output feedback signals, can be detected by different displacement/angle sensors. Although the self-built experimental platform is not as large as practical cranes, it has the main functions of a ship-mounted crane, consisting of boom rotation, rope translation, wave-induced ship motions, payload swing, and so on. Moreover, we have conducted many experiments to test the platform's performance, which show that the platform can satisfactorily reflect the operational principle of ship-mounted cranes.[3] The values of some platform parameters are as follows:

$$m = 0.234 \text{ kg}, \quad L_b = 0.65 \text{ m}$$
$$M_{ob} = 0.29 \text{ kg} \cdot \text{m}, \quad J = 0.2457 \text{ kg} \cdot \text{m}^2.$$

Furthermore, some dead-zone-related parameters are $b_l = -0.5$, $b_r = 0.5$, $g_l(u_i) = u_i + 0.5$, and $g_r(u_i) = u_i - 0.5$. In addition, in order to imitate the ship roll motions, the motion platform (marked in Fig. 3) moves along with the following periodic trajectory:

$$\upsilon(t) = 4\cos(0.6t + 0.6) \text{ deg}. \tag{60}$$

Without loss of generality, we set the initial payload position as $y(0) = 0.65$ m and $z(0) = 0.6$ m, i.e., $\xi_1(0) = 0$ deg, $\xi_2(0) = 0.6$ m, and $\xi_3(0) = 0$, and then, the desired payload position in the NED coordinate frame is selected as $y_d = 13\sqrt{3}/40$ m and $z_d = -0.125$ m, indicating that $\xi_{1d} = 30$ deg, $\xi_{2d} = 0.2$ m, and $\xi_{3d} = 0$ deg.

A. Experiment 1

In Experiment 1, to better verify the control performance of the proposed controller, we choose the sliding mode control (SMC) method in [33] and the nonlinear composite controller in [43] as comparative methods, whose control gains are, respectively, chosen as $k_1 = 12.8$, $k_2 = 1.3$, $\mu = 1.4$ and $k_1 = 18$, $k_2 = 3$, $k_3 = 2.5$, $k_{L1} = 33$, $k_{L2} = 10$, $k_\alpha = 0.2$, $k_\beta = 0.25$, $k_x = 0.8$, and $\sigma = 0.01$ after *careful* adjustments. Additionally, the control/update gains in the presented control scheme are selected as follows:

$$\begin{aligned} &k_1 = 2.5, \quad k_{p1} = 16, \ k_{v1} = 4.3, \ k_{\theta_1} = 3.5 \\ &k_2 = 1.5, \quad k_{p2} = 150, \ k_{v2} = 1.5, \ k_{\theta_2} = 2.1 \\ &\alpha = 0.001, \quad \beta_1 = \beta_2 = 10, \ \gamma_1 = \gamma_2 = 1 \\ &\Pi_1 = 6.02, \quad \Pi_2 = 1.06, \ \Gamma_1 = 9.03, \ \Gamma_2 = 8.82 \end{aligned} \tag{61}$$

which are also used (i.e., do not require retuning) in both Experiments 2 and 3.

As shown in Figs. 4–7, the boom and rope can be rapidly steered toward their desired positions, respectively, by the proposed and comparative control approaches. However, for the boom and rope, there are *unnegligible* up-and-down motions around their equilibrium positions in the comparative experiments. Specifically, for the SMC method [33], obvious overshoots are present for the boom motion. Although the composite controller [43] can achieve a better performance, it is still difficult to completely eliminate positioning errors. In contrast, static positioning errors are *almost nonexistent* by means of the suggested controller. Moreover, by the presented control scheme, the maximum swing angle is *smaller* than 7 deg and the residual swing can be eliminated *within* 5 s during the control process, which are *superior* to those controlled by the comparative methods. Meanwhile, the 2-norm of the output weights W_1 and W_2 and the F-norm of the input weights V_1 and V_2 are drawn in Fig. 5, which are always bounded and finally converge to constant values.

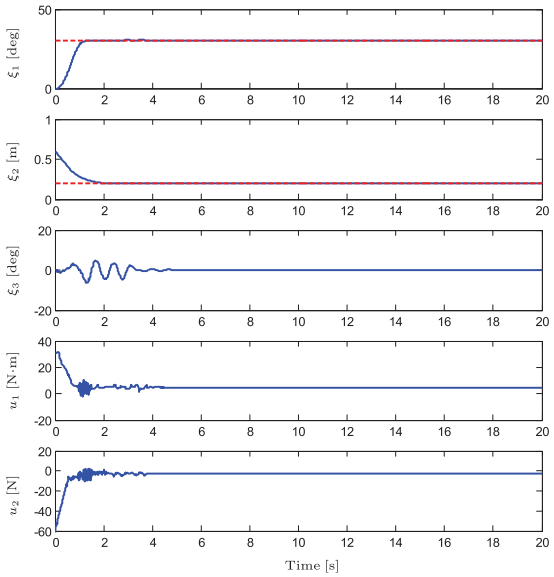

Fig. 4. Experiment 1. The presented control method (red dashed lines: desired positions and blue solid lines: experimental results).

B. Experiment 2

In this experiment, the payload mass is changed to 0.5 kg to validate the robustness of the suggested control approach against parametric uncertainties.

From Fig. 8, it can be observed that even when the payload mass is changed, the presented controller can still provide accurate gravity compensation. Hence, the boom and rope can successfully arrive at the desired positions without unfavorable positioning errors. In contrast, as shown in Figs. 9 and 10, the comparative controllers [33], [43] cannot adapt to the variation of the payload mass; as a result, obvious positioning errors and back-and-forth motions of the boom/rope are exhibited (as shown in the top two subplots in Figs. 9 and 10), which cause obvious residual payload swing and degrade the control performance.

C. Experiment 3

Considering that the payload often suffers from external disturbances in real applications, we purposely perturb the

[3]The video of the crane hardware platform and some experimental results is available at https://youtu.be/8OExn8wwhO0.

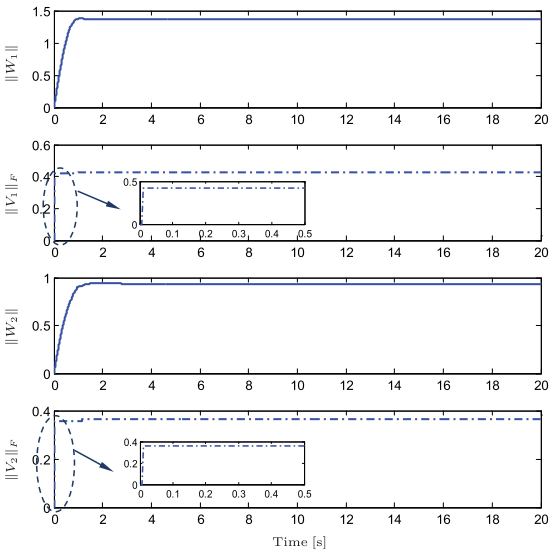

Fig. 5. Experiment 1. The neural network weights (blue solid lines: 2-norm of the output weights W_1 and W_2 and blue dashed–dotted lines: F-norm of the input weights V_1 and V_2).

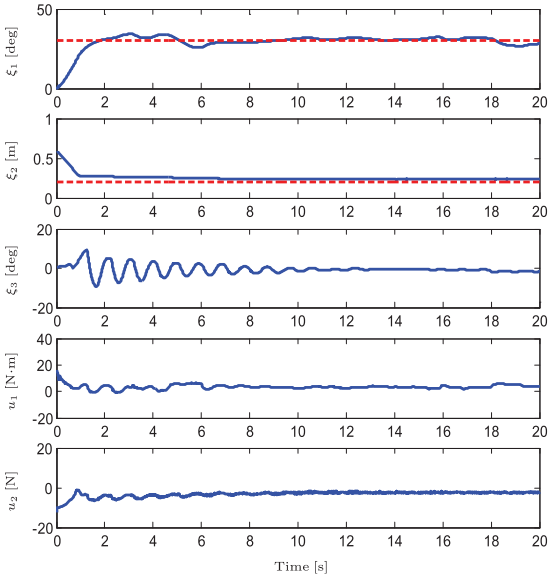

Fig. 6. Experiment 1. The comparative SMC method in [33] (red dashed lines: desired values and blue solid lines: experimental results).

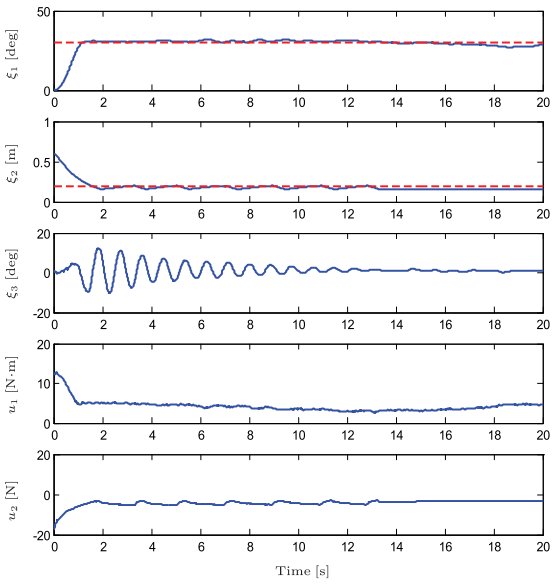

Fig. 7. Experiment 1. The comparative composite control method in [43] (red dashed lines: desired positions and blue solid lines: experimental results).

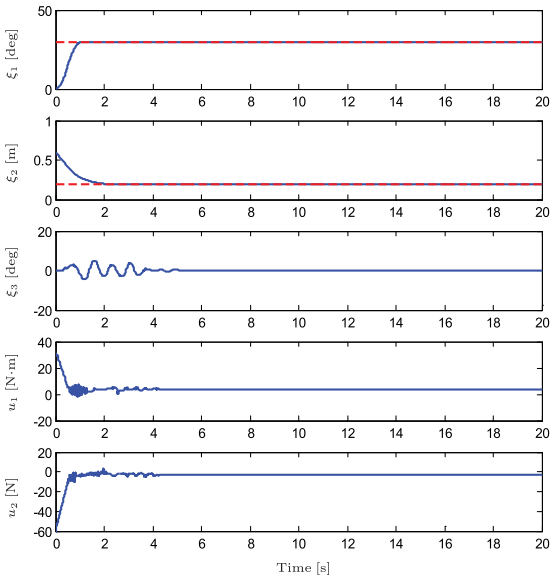

Fig. 8. Experiment 2. The presented control method in case of changed plant parameters (red dashed lines: desired positions and blue solid lines: experimental results).

payload in the control process to induce two kinds of common disturbances, which are detailedly described as follows.

Perturbation 1: Due to artificial perturbations, the initial payload swing angle reaches 9.7 deg, i.e., $\xi_3(0)$ is changed to a nonzero value different from the first two experiments.

Perturbation 2: By adding disturbances to the payload around 12.1 s, the maximum payload swing angle is up to -37.8 deg at about 12.6 s.

The corresponding experimental results are shown in Figs. 11 and 12, respectively. It can be easily seen that the nonzero initial swing angle does not obviously influence the payload swing amplitude, and simultaneously, accurate boom/rope positioning can also be accomplished within 2 s. In addition, from the third subplot in Fig. 12, the additional swing angle caused by external disturbances can be successfully eliminated within 4.3 s by the presented control method, and the ultimate positioning performance of the boom/rope is not impacted either, which illustrates the satisfactory robustness and effectiveness of the presented approach.

D. Experiment 4

In order to fully validate the control performance of the presented controller in the presence of wave-induced loads, the following two groups of experiments are implemented.

Group 1: Irregular wave-induced roll motions of ship-mounted crane systems.

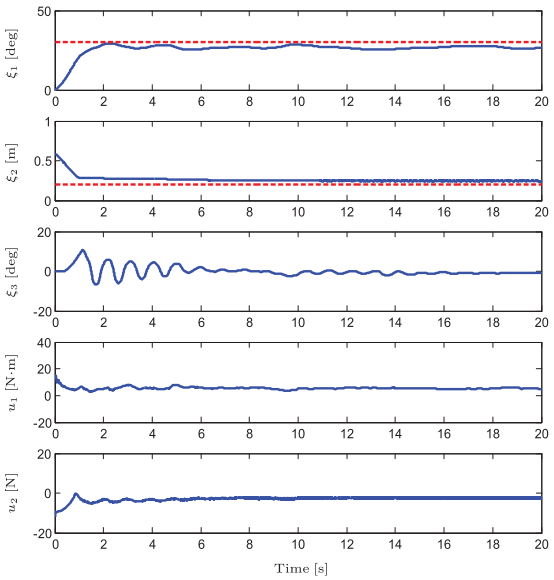

Fig. 9. Experiment 2. The comparative SMC method in [33] in case of changed plant parameters (red dashed lines: desired values and blue solid lines: experimental results).

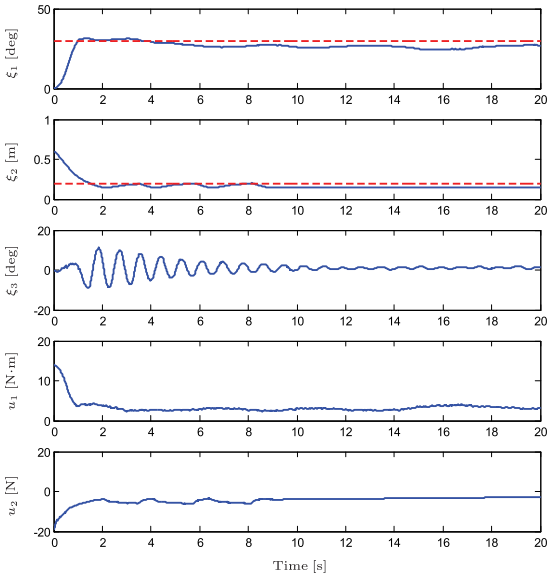

Fig. 10. Experiment 2. The comparative composite control method in [43] in case of changed plant parameters (red dashed lines: desired positions and blue solid lines: experimental results).

Group 2: Irregular wave-induced roll, pitch, and heave motions of ship-mounted crane systems.

In Experiment 4, we utilize the wave-induced motion trajectories calculated by response amplitude operator (RAO) in the Marine Systems Simulator (MSS) toolbox, which are shown in Fig. 13 (including the ship roll, pitch, and heave motions) to replace the periodic cosine motion trajectory in (60). First, we only add the ship roll motions (the first subplot of Fig. 13) into the experimental platform. By comparing Figs. 4 and 14, it can be observed that different roll motions do not have obvious influences on the control performance. In particular, when the roll motions calculated by RAO are introduced into

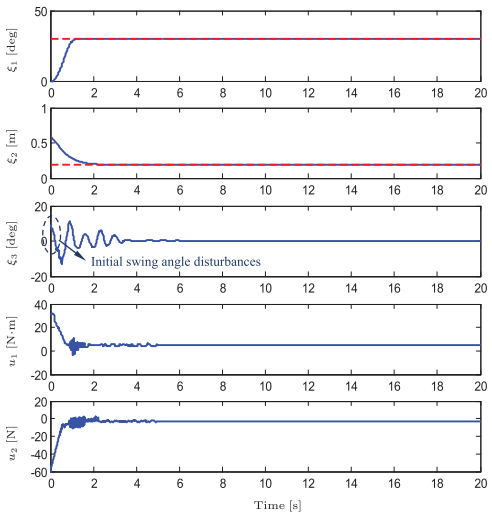

Fig. 11. Experiment 3—Group 1. Initial swing angle perturbations (red dashed lines: desired positions and blue solid lines: experimental results).

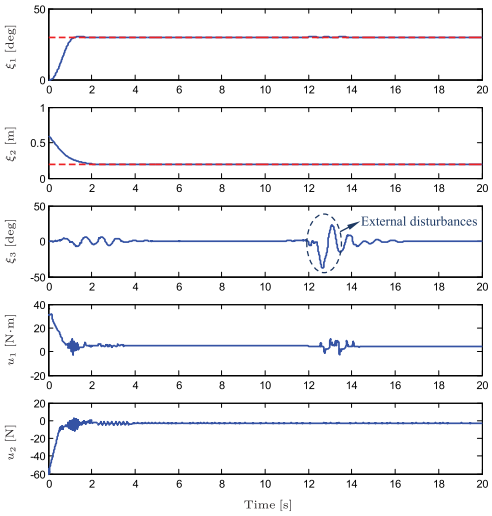

Fig. 12. Experiment 3—Group 2. External disturbances (red dashed lines: desired positions and blue solid lines: experimental results).

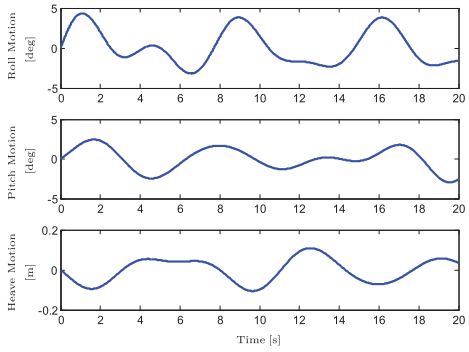

Fig. 13. Experiment 4. The irregular roll, pitch, and heave motion trajectories.

Experiment 4, the boom and rope can still be satisfactorily steered to their destinations; moreover, the payload can be transported to the desired position with negligible residual

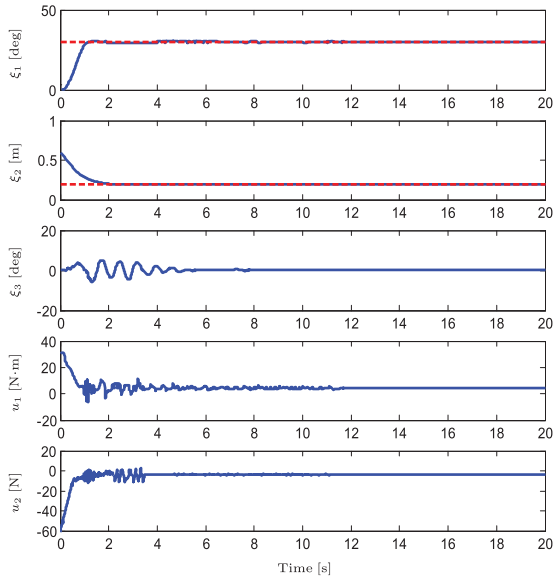

Fig. 14. Experiment 4—Group 1. The presented control method with irregular roll motions (red dashed lines: desired positions and blue solid lines: experimental results).

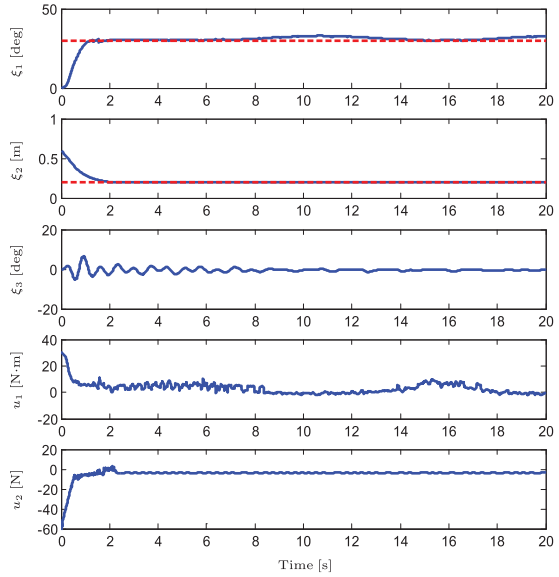

Fig. 15. Experiment 4—Group 2. The presented control method with irregular roll, pitch, and heave motions (red dashed lines: desired positions and blue solid lines: experimental results).

swing, which is consistent with the theoretical analysis of this paper.

In addition, as shown in Fig. 15, even when the pitch and heave motions are exerted on the system, the boom and rope can still be satisfactorily controlled. Moreover, the presented control method can limit the maximum amplitude of the payload within 6.6 deg. It is noticed that, since we do not take the ship pitch and heave motions into account during the controller design, small residual payload swing exists in the later transportation process. In our future work, we will fully consider the influences of ship roll, pitch, and heave motions during the controller design and analysis in order to achieve more effective control for ship-mounted crane systems.

VI. Conclusion

This paper has presented a nonlinear control approach to realize effective control for all state variables of underactuated ship-mounted crane systems. In particular, the boom and rope can reach and then can be stabilized at their desired positions in finite time, respectively. Simultaneously, the payload swing angle can be suppressed, and the corresponding residual swing is also completely eliminated. In particular, in the light of Lyapunov-based techniques, the stability for the equilibrium point of ship-mounted crane systems is proven by a strict theoretical analysis without any linearizing operations for the original complex dynamics. The proposed approach can successfully address the unknown/uncertain parameters/structures in ship-mounted crane dynamics and also the nonlinear input dead zones in servo motors; hence, the robustness of the control system is guaranteed. Finally, a series of hardware experimental results illustrates the effectiveness and practicality of the presented control scheme. Additionally, we will try to implement the experiments on large-scale ship-mounted cranes if the conditions permit in the future.

Appendix
Proof of (27)

Proof: First, we can implement the Taylor expansion for $\sigma(V_1^\top \boldsymbol{x})$ as follows:

$$\sigma\left(V_1^\top \boldsymbol{x}\right) = \sigma\left(\hat{V}_1^\top \boldsymbol{x}\right) + \dot{\sigma}\left(\hat{V}_1^\top \boldsymbol{x}\right)\tilde{V}_1^\top \boldsymbol{x} + O\left(\tilde{V}_1^\top \boldsymbol{x}\right)^2 \tag{62}$$

where $O(\tilde{V}_1^\top \boldsymbol{x})^2$ is the high-order residual term of the Taylor expansion. Then, together with (62), it is easy to calculate that

$$\begin{aligned}
&W_1^\top \sigma\left(V_1^\top \boldsymbol{x}\right) - \hat{W}_1^\top \sigma\left(\hat{V}_1^\top \boldsymbol{x}\right) + \epsilon_1 \\
&= W_1^\top \left[\sigma\left(V_1^\top \boldsymbol{x}\right) - \sigma\left(\hat{V}_1^\top \boldsymbol{x}\right)\right] + \tilde{W}_1^\top \sigma\left(\hat{V}_1^\top \boldsymbol{x}\right) + \epsilon_1 \\
&= W_1^\top \left[\dot{\sigma}\left(\hat{V}_1^\top \boldsymbol{x}\right)\tilde{V}_1^\top \boldsymbol{x} + O\left(\tilde{V}_1^\top \boldsymbol{x}\right)^2\right] + \tilde{W}_1^\top \sigma\left(\hat{V}_1^\top \boldsymbol{x}\right) + \epsilon_1 \\
&= \tilde{W}_1^\top \dot{\sigma}\left(\hat{V}_1^\top \boldsymbol{x}\right)\tilde{V}_1^\top \boldsymbol{x} + \hat{W}_1^\top \dot{\sigma}\left(\hat{V}_1^\top \boldsymbol{x}\right)\tilde{V}_1^\top \boldsymbol{x} \\
&\quad + W_1^\top O\left(\tilde{V}_1^\top \boldsymbol{x}\right)^2 + \tilde{W}_1^\top \sigma\left(\hat{V}_1^\top \boldsymbol{x}\right) + \epsilon_1 \\
&= \tilde{W}_1^\top \dot{\sigma}\left(\hat{V}_1^\top \boldsymbol{x}\right)V_1^\top \boldsymbol{x} - \tilde{W}_1^\top \dot{\sigma}\left(\hat{V}_1^\top \boldsymbol{x}\right)\hat{V}_1^\top \boldsymbol{x} + \tilde{W}_1^\top \sigma\left(\hat{V}_1^\top \boldsymbol{x}\right) \\
&\quad + \hat{W}_1^\top \dot{\sigma}\left(\hat{V}_1^\top \boldsymbol{x}\right)\tilde{V}_1^\top \boldsymbol{x} + W_1^\top O\left(\tilde{V}_1^\top \boldsymbol{x}\right)^2 + \epsilon_1 \\
&= \tilde{W}_1^\top \sigma\left(\hat{V}_1^\top \boldsymbol{x}\right) - \tilde{W}_1^\top \dot{\sigma}\left(\hat{V}_1^\top \boldsymbol{x}\right)\hat{V}_1^\top \boldsymbol{x} \\
&\quad + \hat{W}_1^\top \dot{\sigma}\left(\hat{V}_1^\top \boldsymbol{x}\right)\tilde{V}_1^\top \boldsymbol{x} + \Lambda_1.
\end{aligned}$$

We can also carry out a similar analysis for $W_2^\top \sigma(V_2^\top \boldsymbol{x}) - \hat{W}_2^\top \sigma(\hat{V}_2^\top \boldsymbol{x}) + \epsilon_2$. Hence, (27) is proven. ■

Acknowledgment

The authors would like to thank the Associate Editor and all reviewers for the professional suggestions and comments, which have greatly improved the quality of the presentation.

References

[1] X. He, W. He, J. Shi, and C. Sun, "Boundary vibration control of variable length crane systems in two-dimensional space with output constraints," *IEEE/ASME Trans. Mechatronics*, vol. 22, no. 5, pp. 1952–1962, Oct. 2017.

[2] J. Smoczek and J. Szpytko, "Particle swarm optimization-based multivariable generalized predictive control for an overhead crane," *IEEE/ASME Trans. Mechatronics*, vol. 22, no. 1, pp. 258–268, Jun. 2017.

[3] X. Wu and X. He, "Enhanced damping-based anti-swing control method for underactuated overhead cranes," *IET Control Theory Appl.*, vol. 9, no. 12, pp. 1893–1900, Aug. 2015.

[4] A. T. Le and S.-G. Lee, "3D cooperative control of tower cranes using robust adaptive techniques," *J. Franklin Inst.*, vol. 354, no. 18, pp. 8333–8357, 2017.

[5] M. S. Park, D. Chwa, and M. Eom, "Adaptive sliding-mode antisway control of uncertain overhead cranes with high-speed hoisting motion," *IEEE Trans. Fuzzy Syst.*, vol. 22, no. 5, pp. 1262–1271, Oct. 2014.

[6] A. Piazzi and A. Visioli, "Optimal dynamic-inversion-based control of an overhead crane," *IEE Proc.-Control Theory Appl.*, vol. 149, no. 5, pp. 405–411, Sep. 2002.

[7] T. Vyhlídal, M. Anderle, J. Bušek, and S. I. Niculescu, "Time-delay algorithms for damping oscillations of suspended payload by adjusting the cable length," *IEEE/ASME Trans. Mechatronics*, vol. 22, no. 5, pp. 2319–2329, Oct. 2017.

[8] O. Sawodny, H. Aschemann, and S. Lahres, "An automated gantry crane as a large workspace robot," *Control Eng. Pract.*, vol. 10, no. 12, pp. 1323–1338, Dec. 2002.

[9] S. Garrido, M. Abderrahim, A. Gimenez, R. Diez, and C. Balaguer, "Anti-swinging input shaping control of an automatic construction crane," *IEEE Trans. Autom. Sci. Eng.*, vol. 5, no. 3, pp. 549–557, Jul. 2008.

[10] W. Singhose, L. Porter, M. Kenison, and E. Kriikku, "Effects of hoisting on the input shaping control of gantry cranes," *Control Eng. Pract.*, vol. 8, no. 10, pp. 1159–1165, 2000.

[11] N. Uchiyama, H. Ouyang, and S. Sano, "Simple rotary crane dynamics modeling and open-loop control for residual load sway suppression by only horizontal boom motion," *Mechatronics*, vol. 23, no. 8, pp. 1223–1236, Dec. 2013.

[12] W. Blajer and K. Kolodziejczyk, "Motion planning and control of gantry cranes in cluttered work environment," *IET Control Theory Appl.*, vol. 1, no. 5, pp. 1370–1379, Sep. 2007.

[13] H.-H. Lee, "Motion planning for three-dimensional overhead cranes with high-speed load hoisting," *Int. J. Control*, vol. 78, no. 12, pp. 875–886, Aug. 2005.

[14] W. He, S. Zhang, and S. S. Ge, "Adaptive control of a flexible crane system with the boundary output constraint," *IEEE Trans. Ind. Electron.*, vol. 61, no. 8, pp. 4126–4133, Aug. 2014.

[15] A. M. Abdullahi *et al.*, "Adaptive output-based command shaping for sway control of a 3D overhead crane with payload hoisting and wind disturbance," *Mech. Syst. Signal Process.*, vol. 98, pp. 157–172, Jan. 2018.

[16] N. Sun, Y. Fang, H. Chen, B. Lu, and Y. Fu, "Slew/translation positioning and swing suppression for 4-DOF tower cranes with parametric uncertainties: Design and hardware experimentation," *IEEE Trans. Ind. Electron.*, vol. 63, no. 10, pp. 6407–6418, Oct. 2016.

[17] A. T. Le, S.-G. Lee, and S.-C. Moon, "Partial feedback linearization and sliding mode techniques for 2D crane control," *Trans. Inst. Meas. Control*, vol. 36, no. 1, pp. 78–87, 2014.

[18] C. Vázquez, J. Collado, and L. Fridman, "Control of a parametrically excited crane: A vector Lyapunov approach," *IEEE Trans. Control Syst. Technol.*, vol. 21, no. 6, pp. 2332–2340, Nov. 2013.

[19] M. I. Solihin, M. A. S. Kamal, and A. Legowo, "Objective function selection of GA-based PID control optimization for automatic gantry crane," in *Proc. Int. Conf. Comput. Commun. Eng.*, Kuala Lumpur, Malaysia, May 2008, pp. 883–887.

[20] D. Wang, H. He, and D. Liu, "Intelligent optimal control with critic learning for a nonlinear overhead crane system," *IEEE Trans. Ind. Informat.*, vol. 14, no. 7, pp. 2932–2940, Jul. 2018.

[21] Y. Zhao and H. Gao, "Fuzzy-model-based control of an overhead crane with input delay and actuator saturation," *IEEE Trans. Fuzzy Syst.*, vol. 20, no. 1, pp. 181–186, Feb. 2012.

[22] Z. Ren, R. Skjetne, and Z. Gao, "Modeling and control of crane overload protection during marine lifting operation based on model predictive control," in *Proc. 36th ASME Int. Conf. Ocean, Offshore Arctic Eng.*, Trondheim, Norway, Jun. 2017, p. V009T12A027-.

[23] T. I. Fossen, *Handbook of Marine Craft Hydrodynamics and Motion Control*. Hoboken, NJ, USA: Wiley, 2011.

[24] W. He, Z. Li, Y. Dong, and T. Zhao, "Design and adaptive control for an upper limb robotic exoskeleton in presence of input saturation," *IEEE Trans. Neural Netw. Learn. Syst.*, vol. 30, no. 1, pp. 97–108, Jan. 2019.

[25] Y.-X. Li and G.-H. Yang, "Event-based adaptive NN tracking control of nonlinear discrete-time systems," *IEEE Trans. Neural Netw. Learn. Syst.*, vol. 29, no. 9, pp. 4359–4369, Sep. 2018.

[26] Y. Li and S. Tong, "Adaptive fuzzy output-feedback stabilization control for a class of switched nonstrict-feedback nonlinear systems," *IEEE Trans. Cybern.*, vol. 47, no. 4, pp. 1007–1016, Apr. 2017.

[27] Y.-J. Liu, L. Tang, S.-C. Tong, C. L. P. Chen, and D.-J. Li, "Reinforcement learning design-based adaptive tracking control with less learning parameters for nonlinear discrete-time MIMO systems," *IEEE Trans. Neural Netw. Learn. Syst.*, vol. 26, no. 1, pp. 165–176, Jan. 2015.

[28] K. S. Hong and Q. H. Ngo, "Dynamics of the container crane on a mobile harbor," *Ocean Eng.*, vol. 53, no. 2, pp. 16–24, 2012.

[29] Y. Chu, F. Sanfilippo, V. Æsøy, and H. Zhang, "An effective heave compensation and anti-sway control approach for offshore hydraulic crane operations," in *Proc. IEEE Int. Conf. Mechatronics Autom.*, Tianjin, China, Aug. 2014, pp. 1282–1287.

[30] S. Küchler, T. Mahl, J. Neupert, K. Schneider, and O. Sawodny, "Active control for an offshore crane using prediction of the vessel's motion," *IEEE/ASME Trans. Mechatronics*, vol. 16, no. 2, pp. 297–309, Apr. 2011.

[31] J. Neupert, T. Mahl, B. Haessig, O. Sawodny, and K. Schneider, "A heave compensation approach for offshore cranes," in *Proc. Amer. Control Conf.*, Seattle, WA, USA, Jun. 2008, pp. 538–543.

[32] T. A. Johansen, T. I. Fossen, S. I. Sagatun, and F. G. Nielsen, "Wave synchronizing crane control during water entry in offshore moonpool operations—Experimental results," *IEEE J. Ocean. Eng.*, vol. 28, no. 4, pp. 720–728, Oct. 2003.

[33] Q. H. Ngo and K. S. Hong, "Sliding-mode antisway control of an offshore container crane," *IEEE/ASME Trans. Mechtronics*, vol. 17, no. 2, pp. 201–209, Apr. 2012.

[34] Q. H. Ngo, N. P. Nguyen, C. N. Nguyen, T. H. Tran, and Q. P. Ha, "Fuzzy sliding mode control of an offshore container crane," *Ocean Eng.*, vol. 140, pp. 125–134, Aug. 2017.

[35] M. Agostini, G. G. Parker, K. Groom, H. Schaub, and R. D. Robinett, "Command shaping and closed-loop control interactions for a ship crane," in *Proc. Amer. Control Conf.*, Anchorage, AK, USA, vol. 3, May 2002, pp. 2298–2304.

[36] B. Kimiaghalam, A. Homaifar, and M. Bikdash, "Feedback and feedforward control law for a ship crane with Maryland rigging system," in *Proc. Amer. Control Conf.*, Chicago, IL, USA, vol. 2, Jun. 2002, pp. 1047–1051.

[37] Z. N. Masoud, A. H. Nayfeh, and D. T. Mook, "Cargo pendulation reduction of ship-mounted cranes," *Nonlinear Dyn.*, vol. 35, no. 3, pp. 299–311, 2004.

[38] D. Kim and Y. Park, "Tracking control in $x - y$ plane of an offshore container crane," *J. Vibrat. Control*, vol. 23, no. 3, pp. 469–483, Feb. 2017.

[39] N. Sun, Y. Fang, H. Chen, and B. He, "Adaptive nonlinear crane control with load hoisting/lowering and unknown parameters: Design and experiments," *IEEE/ASME Trans. Mechatronics*, vol. 20, no. 5, pp. 2107–2119, Oct. 2015.

[40] R. R. Selmic and F. L. Lewis, "Deadzone compensation in motion control systems using neural networks," *IEEE Trans. Autom. Control*, vol. 45, no. 4, pp. 602–613, Apr. 2000.

[41] M. C. Turner, "Actuator deadzone compensation: Theoretical verification of an intuitive control strategy," *IEE Proc.–Control Theory Appl.*, vol. 153, no. 1, pp. 59–68, Jan. 2006.

[42] R. M. T. R. Ismail, N. D. That, and Q. P. Ha, "Modelling and robust trajectory following for offshore container crane systems," *Autom. Construct.*, vol. 59, pp. 179–187, Nov. 2015.

[43] Y. Fang, P. Wang, N. Sun, and Y. Zhang, "Dynamics analysis and nonlinear control of an offshore boom crane," *IEEE Trans. Ind. Electron.*, vol. 61, no. 1, pp. 414–427, Jan. 2014.

[44] S. Messineo and A. Serrani, "Offshore crane control based on adaptive external models," *Automatica*, vol. 45, no. 11, pp. 2546–2556, Nov. 2009.

[45] D. Wang, D. Liu, C. Mu, and Y. Zhang, "Neural network learning and robust stabilization of nonlinear systems with dynamic uncertainties," *IEEE Trans. Neural Netw. Learn. Syst.*, vol. 29, no. 4, pp. 1342–1351, Apr. 2018.

[46] B. Xu, "Composite learning control of flexible-link manipulator using NN and DOB," *IEEE Trans. Syst., Man, Cybern., Syst.*, vol. 48, no. 11, pp. 1979–1985, Nov. 2018.
[47] S. Zhang, Y. Dong, Y. Ouyang, Z. Yin, and K. Peng, "Adaptive neural control for robotic manipulators with output constraints and uncertainties," *IEEE Trans. Neural Netw. Learn. Syst.*, vol. 29, no. 11, pp. 5554–5564, Nov. 2018.
[48] Q. Zhou, S. Zhao, H. Li, R. Lu, and C. Wu, "Adaptive neural network tracking control for robotic manipulators with dead zone," *IEEE Trans. Neural Netw. Learn. Syst.*, to be published. doi: 10.1109/TNNLS.2018.2869375.
[49] L. N. Hand and J. D. Finch, *Analytical Mechanics*. Cambridge, U.K.: Cambridge Univ. Press, 1998.
[50] L. Wang, T. Chai, and L. Zhai, "Neural-network-based terminal sliding-mode control of robotic manipulators including actuator dynamics," *IEEE Trans. Ind. Electron.*, vol. 56, no. 9, pp. 3296–3304, Sep. 2009.
[51] W. He, A. O. David, Z. Yin, and C. Sun, "Neural network control of a robotic manipulator with input deadzone and output constraint," *IEEE Trans. Syst., Man, Cybern., Syst.*, vol. 46, no. 6, pp. 759–770, Jun. 2016.
[52] D. Xu, D. Zhao, J. Yi, and X. Tan, "Trajectory tracking control of omnidirectional wheeled mobile manipulators: Robust neural network-based sliding mode approach," *IEEE Trans. Syst., Man, Cybern. B, Cybern.*, vol. 39, no. 3, pp. 788–799, Jun. 2009.
[53] H. K. Khalil, *Nonlinear Systems*, 3rd ed. Englewood Cliffs, NJ, USA: Prentice-Hall, 2002.
[54] E. D. Sontag, "Remarks on stabilization and input-to-state stability," in *Proc. 26th Conf. Decision Control*, Tampa, FL, USA, Dec. 1989, pp. 1376–1378.

Tong Yang received the B.S. degree in automation from Nankai University, Tianjin, China, in 2017. She is currently pursuing the Ph.D. degree in control science and engineering, under the supervision of Dr. N. Sun, with the Institute of Robotics and Automatic Information Systems, Nankai University.

Her current research interests include the nonlinear control of underactuated systems, including rotary cranes, offshore cranes, and tower cranes.

Ning Sun (S'12–M'14) received the B.S. degree in measurement and control technology and instruments from Wuhan University, Wuhan, China, in 2009, and the Ph.D. degree in control theory and control engineering from Nankai University, Tianjin, China, in 2014.

He is currently an Associate Professor with the Institute of Robotics and Automatic Information Systems, Nankai University. His current research interests include underactuated systems, such as cranes, and nonlinear control with applications to mechatronic systems.

Dr. Sun received the First Class Prize of the Natural Science Award from the Chinese Association for Artificial Intelligence (CAAI), the First Class Prize of the Tianjin Natural Science Award, the Golden Patent Award of Tianjin, the IJCAS Academic Activity Award, the Outstanding Ph.D. Dissertation Award from the Chinese Association of Automation (CAA), and the Japan Society for the Promotion of Science (JSPS) Postdoctoral Fellowship for Research in Japan (Standard). He is the Executive Editor of *Measurement and Control* and serves as an Associate Editor (Editorial Board Member) for several journals, including the IEEE ACCESS, the *International Journal of Control, Automation, and Systems*, the *International Journal of Precision Engineering and Manufacturing*, the *International Journal of Advanced Robotic Systems*, *Information Technology and Control*, and *Advances in Mechanical Engineering*.

He Chen received the B.S. degree in automation from Nankai University, Tianjin, China, in 2013, where he is currently pursuing the Ph.D. degree in control science and engineering with the Institute of Robotics and Automatic Information Systems.

His current research interests include control of mechatronics, overhead cranes, and wheeled mobile robots.

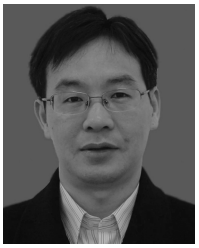

Yongchun Fang (S'00–M'02–SM'08) received the B.S. degree and the M.S. degree in control theory and applications from Zhejiang University, Hangzhou, China, in 1996 and 1999, respectively, and the Ph.D. degree in electrical engineering from Clemson University, Clemson, SC, USA, in 2002.

From 2002 to 2003, he was a Post-Doctoral Fellow with the Sibley School of Mechanical and Aerospace Engineering, Cornell University, Ithaca, NY, USA. He is currently a Professor with the Institute of Robotics and Automatic Information Systems, Nankai University, Tianjin, China. His current research interests include nonlinear control, visual servoing, control of underactuated systems, and atomic force microscope (AFM)-based nanosystems.

Dr. Fang received the National Science Fund for Distinguished Young Scholars of China in 2013. He is a Distinguished Professor of the Changjiang Scholars Program.